Bulletin of Engineering Geology and the Environment (2022) 81:457
https://doi.org/10.1007/s10064-022-02962-y

ORIGINAL PAPER

Thermomechanical characterization of two Jalore granites with different grain sizes for India's HLW disposal

Pradeep Kumar Gautam[1,3] · Suraj Pratap Singh[1] · Amar Agarwal[1] · Trilok Nath Singh[2]

Received: 14 March 2022 / Accepted: 26 September 2022 / Published online: 4 October 2022
© Springer-Verlag GmbH Germany, part of Springer Nature 2022

Abstract

The time-dependent temperature distributions in the deep geological repository must be carefully designed for high-level radioactive waste (HLW). Therefore, for the main purpose of this study, we carried out a laboratory investigation of the physical and mechanical properties of the two Jalore white and red granitic rocks with variable grain sizes at different heating rates (3, 5, 10, and 15 °C/min). After heat treatments, micro- and macrocracks are readily observed in coarse-grained red granite, whereas no significant cracks were observed in fine-grained white granite. As heating rates increased, the number of intergranular cracks in the red and white granite increased. When the heating rate was more than 10 °C/min, in coarse red granite specimens, separate grains can be observed and the tensile mode of failure was dominated by thermally induced cracks. Microscopic observations revealed mainly intergranular microcracks in quartz, the opening of cleavage plains, and deformation in biotite in red granite due to mismatched thermal expansion. Biotite produces a concentration of stresses along its grain boundaries. In contrast, the thermal expansion anisotropy of quartz, the microstructure of rocks with large amounts of quartz, does not necessarily experience large stresses in white granite. Increases in tensile strength were less significant for coarse-grained red granite specimens than for fine-grained white granite specimens. The results can be used to identify the deformation and failure analysis of host rock for India's HLW disposal sites.

Keywords Nuclear waste repository · Jalore granitoid · Different heating rates · Microstructure · Tensile strength · Cohesion-weakening-friction-strengthening (CWFS)

Introduction

Policymakers and researchers seek to reduce carbon emissions to combat the harmful effects of climate change, the impetus to shift away from fossil fuel–based power industries. The estimated presence of fossil fuels will be exhausted by the year 2050 if the present consumption rates continue. Therefore, nuclear power is the alternative option for preventing global warming and is essential to achieving climate change objectives. Many countries have used nuclear power since 1942 because it is reliable, cheap, and environmentally friendly. However, the nuclear power industry expands the question of safe and secure disposal of spent fuel which is required to be identified. Due to the short energy release and a short half-life of low- and medium-level radioactive wastes, they can be easily disposed of, whereas the high-level radioactive waste is very difficult to dispose. The nuclear power industry has spent decades trying to find a solution to dispose of high-level radioactive wastes. Several scientific and technical organizations have recommended a deep geological repository (DGR) as the preferable solution to this issue (IAEA 2009; Wang 2010); Birkholzer et al. 2012), which separates high-level radioactive waste (HLW) from the biosphere by burying it 500 ~ 1000 m in the nuclear waste repository (NWR). The main challenge is effectively isolating the waste from the biosphere for hundreds of thousands of years (Bäckblom and Martin 1999; Hudson et al. 2009, 2011; Tsang et al. 2012). But the long-term performance of repositories of nuclear waste to be deposited in these facilities has remaining significant uncertainties.

✉ Pradeep Kumar Gautam
pgautam.embedded@gmail.com

[1] Applied Structural Geology Group, Department of Earth Sciences, Indian Institute of Technology Kanpur, Kanpur, India

[2] Department of Earth Sciences, Indian Institute of Technology Bombay, Mumbai, India

[3] Civil and Environmental Engineering, Colorado School of Mines, Golden, United States

The KBS-3 V method is one of the proposed models for deep geological disposal of HLW by the Swedish Nuclear Fuel and Waste Management Company (SKB) as shown in Fig. 1a (Backers et al. 2014). The HLW will be encapsulated in copper canisters and deposited vertically in deposition holes, after which the canisters will be embedded in a buffer of compacted bentonite clay, and lastly, the deposition galleries will be excavated to a depth of about 500 m.

Thus, the major key issue is the dimensioning design and safety assessment of the repository for the heat decay process from the placement of canister in the near field. During the decay process, radioactive elements in high-level radioactive wastes release a large amount of heat, which raises the temperature of the rocks surrounding the repository. The rock temperature around nuclear waste in conventional storage cannot exceed 300 °C (Sizgek 2004; Dwivedi et al. 2008). In the case of non-conventional or direct disposal of nuclear waste, the rock temperature may sometimes exceed the rock's melting point (Heuze 1981). As a result, during radionuclide decay, an amount of heat is generated which heats the host rock mass surrounding and the disposal site and increases cracks. Cracks triggered by decay heat are likely to increase the thermal cracking of the host rock. Then, radionuclides may migrate through thermal cracks and those that have been produced by thermal stress. Therefore, it is of great importance to study the thermomechanical properties and damage characteristics of host rock to provide support for high-level waste disposal engineering. Hence, Fig. 1b is the repository configuration and the dimensions are based on the Indian pit mode HLW reference disposal site repository (Dutt et al. 2012; Verma et al. 2015; Maheshwar et al. 2015), while the time-dependent temperature distribution and heat emission curves are in Fig. 1c (Sizgek 2004). According to Sizgek (2004), after a period of surface cooling, all the temperatures remain below 330 °C, which plays an important role in the long-term safety of HLW disposal engineering. The preceding data reveals that rock temperatures rarely reach 300 °C in most nuclear waste repository operations. Many countries have suggested crystalline rocks, such as granite as a potential HLW repository deposit because of their low permeability, high solidity, and strong excavation stability (Zhao et al. 2016; Zuo et al. 2017).

Thus, another key issue is that progressive deformation and failure characteristics are not well understood in brittle rocks, because the strength of intact rock is made up of two components, cohesion and friction. The cohesion and friction components of the failure envelope play a crucial role in determining the stability near subsurface underground openings in these conditions since stresses are generally much higher. As a result, excavation of underground openings often leads to instability and damage to the rock mass adjacent to the opening. Therefore, excavation-induced responses in brittle bedrock are extremely serious under high in situ stresses and brittle failure is frequently observed in deep sparsely crystalline rock masses. Hence, the researchers have shown that brittle rocks encounter five distinct stages during a conventional compression test using the ISRM-recommended procedures, as seen in Fig. 1d. Stage I involves the closure of existing cracks under relatively low loads, resulting in a low initial stiffness. Stage II begins with linear elastic

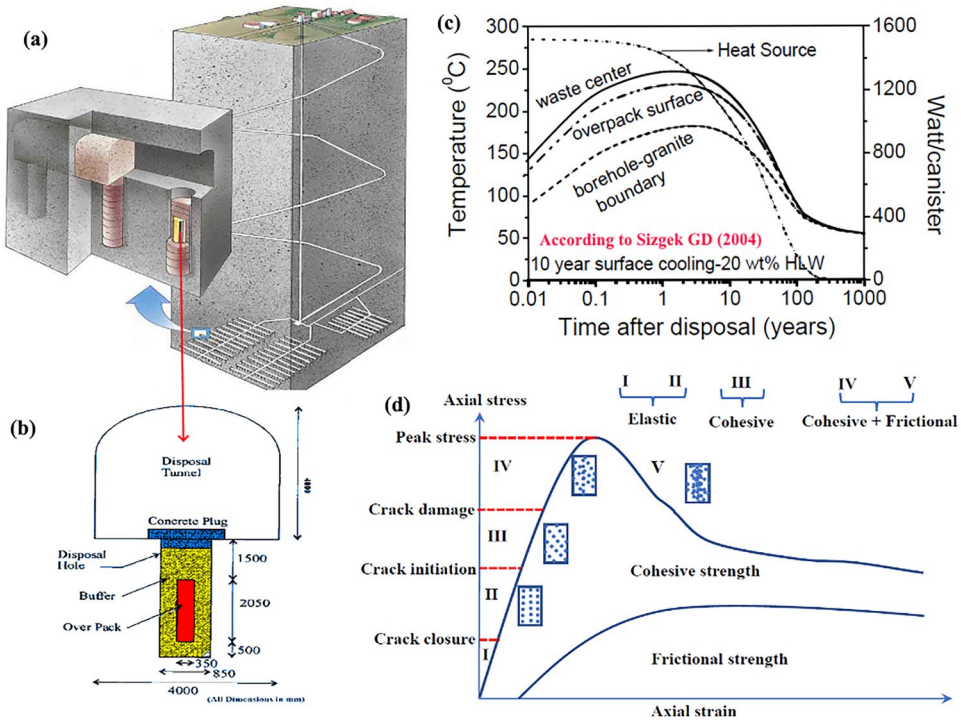

Fig. 1 **a** Schematic illustration of HLW KBS-3 V repository (SKB 2004). **b** Concept proposed for Indian pit mode HLW disposal system (Verma et al. 2015). **c** Heat decay problem in a high-level radioactive waste repository (according to Sizgek (2004)). **d** Strain-dependent mobilization of strength components (cohesive and frictional strength), Modified after Haji-abdolmajid et al. (2003)

deformations in both the axial and lateral axes after crack closure. In stage III, stable axial cracks are started, resulting in a lateral deviation from linear growth. With continued loading, the length and quantity of microcracks inside the rock material increase to the point where axial microcracks coalesce and form shear cracks. Stage IV is unstable crack propagation, and the stress level associated with it is referred to as crack damage stress (Renani and Martin 2018). This suggested model for the brittle failure of rocks is based on cohesion weakening and friction strengthening (CWFS) revealed by Hajiabdolmajid et al. (2003). The CWFS model can reflect both the formation and stabilization of breakout zones around underground openings in hard brittle rocks.

Lin (2002) observed the Inada granite's microcrack density exhibits increasing trends which increase mass exponentially between 20 and 600 °C, meaning that the cumulative amount of newly generated microcracks and the opening of pre-existing microcracks showed distinctly at temperatures between 125 and 200 °C. Chaki et al. (2008) investigated granite specimens exposed to various temperature treatments ranging from 105 to 600 °C and observed that the porosity increased but the gas permeability and the longitudinal wave velocity dropped as the temperature increased. Shao et al. (2014) conducted unconfined compressive strength tests on fine, medium, and coarse grain granite specimens, after heating the specimens to four different temperature values (200, 400, 600, and 800 °C). The results reveal that peak strength and elastic modulus declined as the holding temperature exceeded 400 °C. Fine-grain granites showed lower failure strains at 800 °C, whereas medium- and coarse-grained granites showed higher failure strains. The increased crack density was attributed to thermal crack development during the cooling process for the specimens heated to higher temperatures. Liu and Xu (2015) reported that 600 °C is a critical temperature for the brittle-ductile transition of the stress-strain curve in granite. The results demonstrate that its ductility is much enhanced, and strain can still increase slowly after reaching the peak stress compared to the lower temperature granite samples. Zhao (2016) simulated the process of thermally induced micro- and macrocracks in granite using a particle-based technique. They observed that during the heating process, sparsely dispersed microcracks appeared once the temperature reached 200 °C, with the number of microcracks growing continually as the temperature rose from 200 to 400 °C. Kumari et al. (2017) reported that cohesion and friction angle increased with temperature in the range of 20 to 300 °C, and they related cohesion strengthening to thermally induced expansion causing higher mutual attraction within individual minerals. Chen et al. (2017) demonstrated that the permeability of Beishan granite specimens increased linearly with crack volumetric strain when heated from 100 to 800 °C. SEM photographs of Beishan granite after heat treatment were reported by Zhao et al. (2018). When compared to the 105 °C results, some microstructural alterations can be seen at 200 °C. They also observed that the maximum widths of microcracks in specimens treated at 300 °C and 400 °C are below 2 μm, but for 550 °C (4 μm) and 650 °C (8 μm), the maximum widths increase significantly. This leads to higher permeability in the coarse-grained granite at high temperatures and high pressures. Experimental results indicate clearly how thermally induced cracks increase microcracks and modify permeability and porosity (Wang et al. 2013; dos Santos et al. 2011; Yang and Hu 2018; David et al. 1999; Wang 2014; Nasseri et al. 2007), reduce the modulus of elasticity of the rock (Huang and Xia 2015; Fan et al. 2017; Gautam et al. 2018a, b), and reduce the uniaxial strength (Nasseri et al. 2009; Gautam et al. 2016a, b; Isaka et al. 2018; Rathnaweera et al. 2018; Rong et al. 2018; Li and Ju 2018; Wu et al. 2019; Peng et al. 2016, 2019; Fan et al. 2018). Yin et al. (2021) compared fine-grained granite with coarse-grained granite to conclude that larger grains and extreme heterogeneity in coarser granites cause greater thermal deformation and degradation of mechanical properties.

Therefore, we can conclude that generally, thermal-induced microcracks of granite begin to occur between 300 and 600 °C, and then develop continuously as temperature increases. It is noteworthy that all these investigations were generally conducted with two objectives, as follows: one was to examine the effect of temperature on rock physical properties, and another was to investigate rock thermal cracking behavior. However, there are two types of thermal cracking in rocks. The first is called intergranular cracking, which is caused by a mismatch in the thermal expansion anisotropy of adjacent minerals, leading to broken grain boundaries. The second type is intragranular cracking, which relates to cracking within a grain because of the temperature gradient. The degradation of strength with increasing temperature has always been attributed to thermal cracking caused by inhomogeneous thermal stress, and chemical and physical reactions (mineral phase transition) during and after thermal treatment. The different heating rates based on grain size heterogeneity have not been fully understood and they are summarized in Table 1. All the above work has been done to investigate the thermomechanical properties of rocks at high temperature, i.e., $\leq$ 800 °C, treatment above the damage threshold temperature for deep geothermal energy and fire accident or other high-temperature application. But the strength and deformation behavior of rock under elevated temperatures or after thermal treatment below the damage threshold ($\geq$ 300 °C) have not been comprehensively studied yet. The influence of the heating rate of thermal treatment on rocks has gradually attracted the attention of researchers and engineers. Therefore, the main objective of this is to study the thermomechanical and damage characteristics of host rock to provide support for high-level waste

Table 1 Characteristics of the reviewed rocks of granite under temperature or after temperature during different heating rate treatments

Rock-type (region)	Thermal treatment			References
	Temperature conditions	Temperature range	Heating rate (°C/min)	
Indian granite	Under temperature	20–400 °C	2 and 5 °C/min	Ramana and Sarma (1980)
Westerly granite	Under temperature	20–120 °C	0.4, 1.1, 2.5, 5.0, 10.0, and 12.5 °C/min	Yong and Wang (1980)
Beishan granite	After temperature	100–800 °C	1, 3, 5, 8, 12 and 15 °C/min	Chen et al. (2017)
Central Aare granite	After temperature	20–650 °C	0.17, 5, and 20 °C/s	Rossi et al. (2018)
Eibenstock granite	Under temperature	20–800 °C	5, 200, and 300 °C/min	Wang et al. (2019)
Changsha granite	After temperature	400 °C and 600 °C	1, 2, 4, 6, 10, 20, 30, and 40 °C/min	Shu et al. (2022)
Jalore granitic rocks	After temperature	20–300 °C	3, 5, 10, and 15 °C/min	Present study

disposal engineering aspects. In this study, we investigated the physical and mechanical properties of the two types of Jalore granitoid after different heating rates. The specimens were heated to 300 °C at different heating rates (3, 5, 10, and 15 °C/min) and maintained at each temperature for 12 h. Then, to avoid thermal shock, the specimens were cooled in the furnace to room temperature at 0.57 °C/min. The strain-dependent-based brittleness index (BIε) is also introduced to the entire stress-strain curve (pre- to post-peak stages). The results can be used to measure the deformation and failure properties, and to improve the deep understanding of host rock (granite) for India's HLW deposit.

Materials and methods

Material properties

The surface outcrop granitoid samples used in this experiment were obtained in Jalore district, Rajasthan. This is the most potential site for high-level radioactive waste disposal in India. Two types of Jalore granitoid rocks (white and red granites) were chosen for this research as shown in Fig. 2. Its color-coded test samples are designated as red granite ("RG") and white granite ("WG"). The natural density of red and white granite is about 2.64 and 2.69 g/cm^3 and the P-wave velocity is about 5812 m/s and 5421 m/s, respectively. The red granite ("RG") is a coarse-grained syenogranite with a heterogeneous grain size of ≈12 mm. The mineralogical composition of RG measured by XRD at room temperature (25 °C) was 24.8% quartz, 29.1% plagioclase, 38.2% k-feldspar, and 7.9% biotite mica. The microscopic observation of the Jalore granitoid is shown in Fig. 3. RG contains a larger percentage of k-feldspar and a lower quartz content than plagioclase. Idiomorphic feldspars have straight grain boundaries, while quartz has both straight and interlobate grain boundaries. The k-feldspars have a red color, providing the whole rock with a red appearance. In quartz, "RG" contains subhedral to anhedral crystals with irregular boundaries. The ratio of muscovite to biotite is around 2:1, and they have an elongate flaky shape orientation. The majority of cracks are intergranular, taking advantage of mica boundaries (Sajid et al. 2016; Yılmaz et al. 2011). The white granite ("WG") is metamorphosed in orthogneiss with a very fine grain size of (≈1 mm). The mineralogical composition of WG measured by XRD at room temperature (25 °C) was 38.6% quartz, 32.2% plagioclase, 26.6% k-feldspar, and 4.6% biotite mica. The "WG" shows the interlocking of irregular grains caused by metamorphic processes. The mineral composition of "WG" is mostly composed of white quartz and feldspar minerals. All minerals vary in shape from subhedral to euhedral. The majority of cracks are intergranular and correspond to mica boundaries (Sajid and Arif 2015; Guo and Wong 2020).

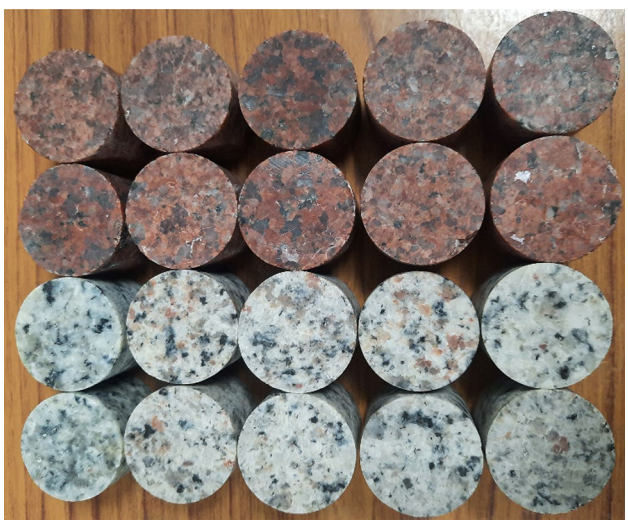

Fig. 2 Photograph of tested specimens of Jalore granitoid

Sample preparation

For the tensile test, the granitoids were cut into disk specimens with a nominal diameter of 30 mm and a thickness of 21 mm (i.e., a ratio of thickness to diameter lesser than 0.7) as per the International Society for Rock Mechanics

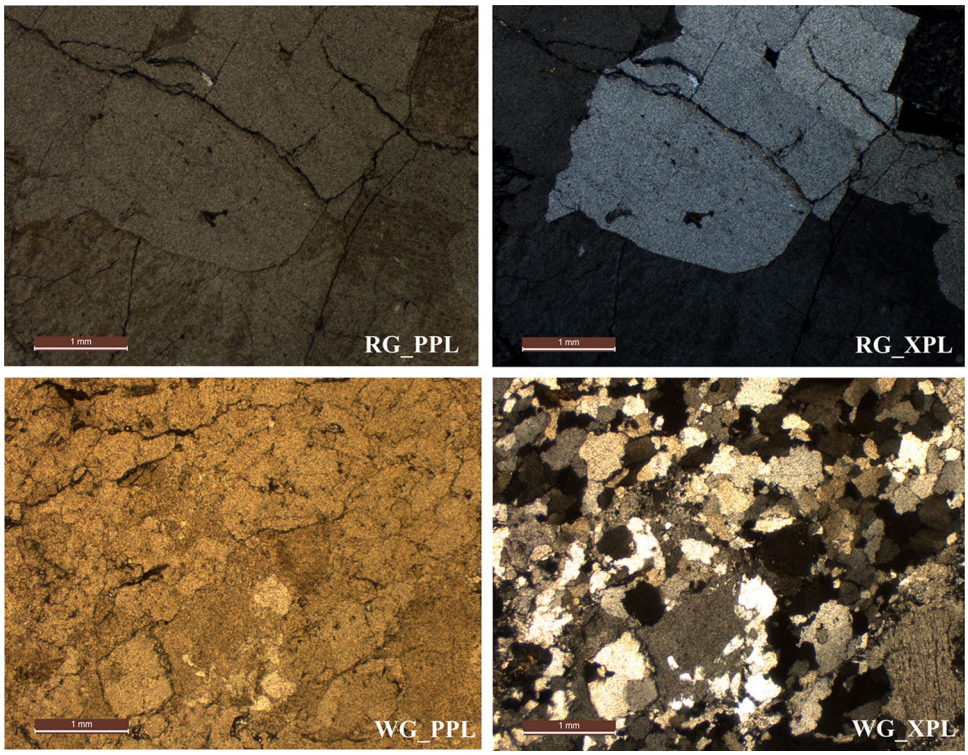

Fig. 3 Microphotographs of the Jalore granitoid

and Rock Engineering (ISRM 1978) standard. The finished specimens' ends were ground flat and parallel to ensure flatness and parallelism of less than 0.05 mm and 0.02 mm, respectively. Twenty specimens of Jalore granitic rocks were investigated to determine their physical and mechanical properties; two sets for each Jalore granitic rock (white and red) were conducted after thermal treatment with various heating rates. All specimens were soaked in water for 1 h before the experiment and then air-dried for 24 h at 105 °C.

Experimental techniques

The split tensile test is an indirect way of evaluating the tensile test carried out at ACMS (Advanced Centre for Materials Science) IIT Kanpur using a screw-driven testing Instron-1195 system as shown in Fig. 4a. The maximum load capacity of the system is 100 kN with an accuracy of 0.01 kN and a crosshead speed (strain rate) minimum of 0.005 mm/min. Closed-loop control of screw-driven test equipment is performed using hardware and software components. A compression loading frame, an axial loading system, and a data collection system make up the direct compression testing machine. Furthermore, signal conditioning and an acquisition device connected to a computer make up the data acquisition system. Data is computer-controlled and collected on all channels using multiple or single data collection methods. In this investigation, the specimens were compressed in a velocity-controlled manner at a displacement rate of 0.1 mm/min until failure occurred. The split tensile test is an indirect way of evaluating the tensile strength in this study. A disk specimen is laid horizontally, and the force is applied to the disk radially on the surface which causes the formation of a vertical crack in the specimen along its diameter.

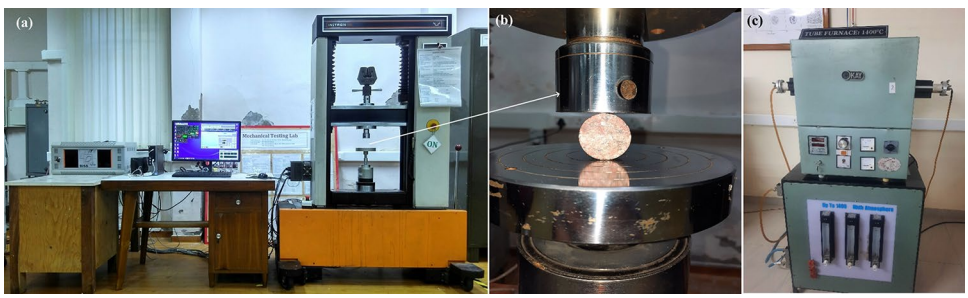

Fig. 4 **a** Photograph of direct loading compression and data acquisition system. **b** Specimen arrangement of indirect splitting tension test. **c** Tube-type high-temperature furnace

The experimental setup for this test is shown in Fig. 4b. Tensile strength increases with the increase in radial compressive force and specimens deteriorate along the direction of the applied force. The heating device is a tube-type high-temperature furnace that consists of a control box and a furnace, as seen in Fig. 4c, which consists of a smart controller, and is designed to have a rated power of 5 kW, a maximum temperature of 1400 °C, a minimum heating rate of 3 °C/min, and a maximum heating rate of 15 °C/min. To investigate the thermomechanical properties of all granitic specimens, different heating rates of 3, 5, 10, and 15 °C/min were used in the tube furnace to heat the specimens from room temperature to 300 °C, as shown in the temperature-time profile in Fig. 5. The thermocouple data logger was used to verify that the rock specimens reached and maintained their proposed set temperature (300 °C) for 12 h. After turning off the tube furnace, the heated samples were kept within the tube furnace to cool from 300 °C to room temperature (around 9 h at a cooling rate of 0.57 °C/min). The cooling rates used to measure the testing specimens were maintained low to minimize thermal shock and to ensure that the thermal cracks in the rock specimens were caused only by the effect of the varying thermal gradient.

An X-ray fluorescence (XRF) spectrometer was used to assess the chemical composition of granite. A wavelength spectrometer is included in the chemical analysis (the model and supplier are Rigaku Corporation, Japan). Powder X-ray diffraction (XRD) was used to determine the mineralogical composition of granite. The PANalytical X'PERT Pro X-ray Diffractometer equipment was used to do the XRD test, which used Cu Ka radiation with a wavelength of 1.5418 Å and a scattering angle of 5° to 80° with a 0.05° step. The tube current and operational voltages were 40 kV and 40 m, respectively. Small blocks (5 mm × 10 mm × 5 mm) were made from the failed

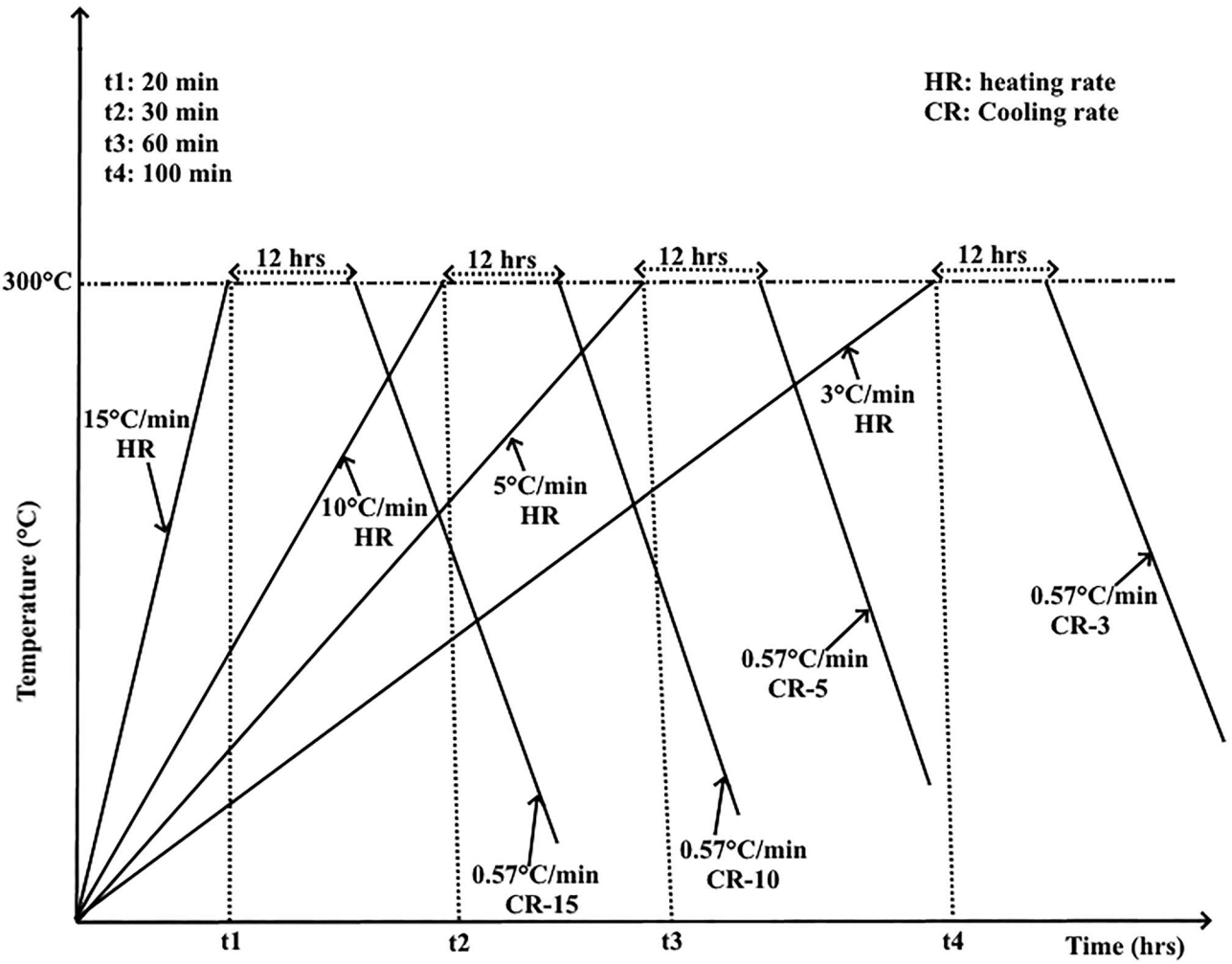

Fig. 5 Temperature-time profile of granitic rocks during different heating rates

samples after the tensile testing. These granite blocks were subjected to scanning electron microscopy (SEM) examinations with CARL ZEISS EVO 50 setup. Additionally, the elemental compositions were determined also using energy-dispersive X-ray spectroscopy (EDX). The SEM image of each sample was taken at different magnifications (1.0K×, 5.0K×, and 10.0K×) to observe the specimen surface morphology. A DIL 805A/D dilatometer (made by Bähr Thermo Analysis GmbH, coupled with an LVDT type measuring head with a resolution of 0.057 mm) was used to determine the thermal expansion and thermal strain of Jalore granitic. Four red and white granite samples, each measured 5 mm in diameter and nominally 20 mm in length, were heated to 300 °C at rates of 3, 5, 10, and 15 °C/min to estimate their linear thermal expansion coefficient and thermal strain.

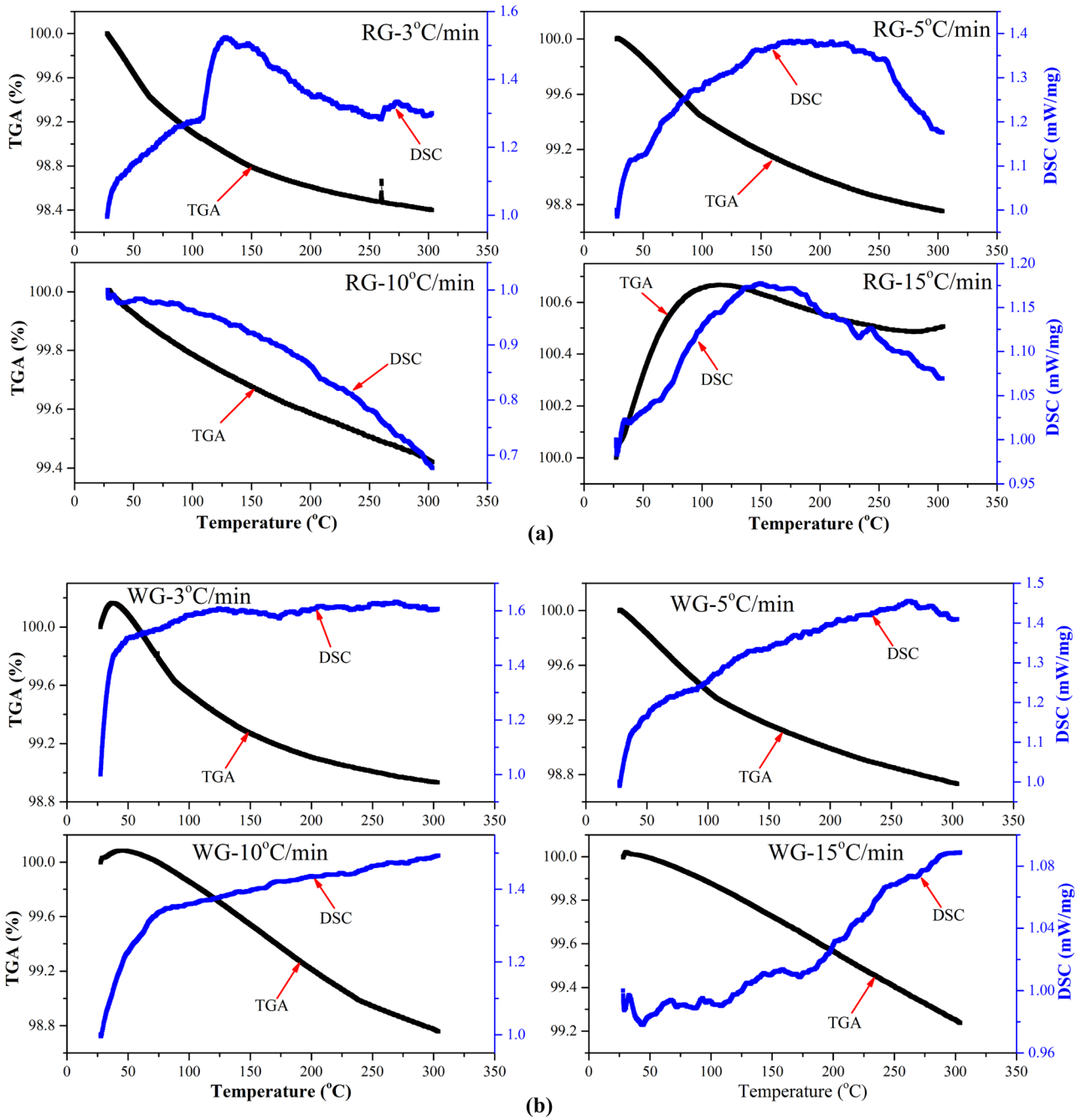

Fig. 6 The variation of DSC and TGA curve of **a** red granite and **b** white granite

Results and discussion

Variation of TGA/DSC and mass loss rate

The results of the thermal analysis of Jalore granitoid (differential scanning calorimetry (DSC) and thermogravimetric analysis (TGA) curve) at different heating rates are presented in Fig. 6. However, TGA and DSC analysis experiments to identify the changes in material composition, with the control experiments conducted as a function of time and temperature. TGA analysis was used to measure the changes in a rock mass with temperature and DSC analysis determined the difference in heat flow rate between a heated sample and the control reference material. The mass of each powdered sample was 21.18 mg for RG and 26.06 mg for WG during these experiments, with a heating rate of 3, 5, 10, and 15 °C/min, with a target temperature of 300 °C. The experiment was carried out in an air atmosphere. The TGA curve shows that at different heating rates between 25 and 300 °C, the rock mass was reduced by 1.6%, 1.2%, and 0.57% at 3, 5, and 10 °C/min, but increased by 0.50% at 15 °C/min for red granite (shown in Fig. 6a), even though white granite has low permeability and high solidity than red granite because the mass constantly decreases by 1.06%, 1.26%, 1.22%, and 0.74% at 3, 5, 10, and 15 °C/min as shown by the TGA curve (shown in Fig. 6b). There are no endothermic/exothermic peaks visible in the DSC curves throughout the 300 °C temperature range. However, the mineral composition and structural characteristics of rock are intrinsic factors that influence the thermal and physical properties of the rock. The initial rock mass loss may be due to the water escaping which is one of the most essential aspects. Notable is the fact that there are three forms of water present in rocks: attached water, chemically water, and mineral mixed bound water. Generally, attached bound water will escape between 70 and 120 °C. Due to the rock's mineral surface gravity, attached bound water can only escape at temperatures over 120 °C. Chemically bound water can entirely escape at about 150 °C, whereas weakly bound water can only escape at around 200–300 °C. Mineral mixed bound water is classified as constitution water, crystal water, and zeolite water. Mineral crystalline lattice water occurs in the form of OH- or H+ and is difficult to separate from the crystal lattice. However, at 400 °C, particularly 450–500 °C, OH- and H + dissociate from the mineral framework and precipitate as water molecules, destroying the mineral framework and forming a new mineral. Crystal water vaporizes at less than 400 °C. Loss of constitution and crystal water could damage the mineral crystalline structure, but not the loss of zeolite water (Zhang et al. 2016; Gautam et al. 2021).

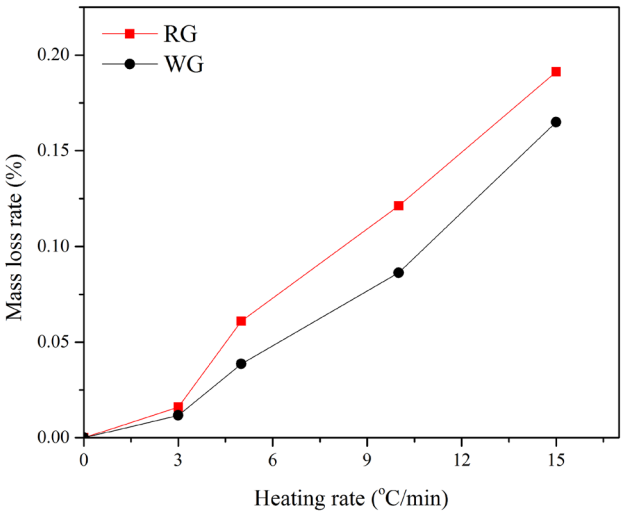

Fig. 7 Variation of mass loss rate

On the other hand, in natural or unheated conditions, the macroscopic mass loss rate of Jalore granitic rock samples was calculated before and after heating treatment as shown in Fig. 7. The mass loss rate properties of rocks reflect changes in internal microvoids, mineral composition, and porosity, implying that they may reveal the variation in internal structure caused by different heating rates. Mass loss rate L_m was determined to interpret the change in mass loss after thermal treatment. L_m can be calculated by Eq. (1) given below; whereas m_o is the initial mass, m_T is the mass after heating (Shi et al. 2020).

$$L_m = \frac{\left(m_o - m_T\right) * 100}{m_o} \tag{1}$$

Variation of the stress-strain curve

The stress-strain comparison curve is obtained during the indirect tension test of Jalore granitoids as shown in Fig. 8. The results reveal that heating rate has a significant influence on stress-strain relations. The stress-strain curve in the compaction phase grows and moves to the right, and the failure strain increases significantly. Then, the bearing capacity falls as a result of the change in the overall stress-strain curve shape at a below 5 °C/min treatment. At 10 °C/min heat treatment in red granite, the slope of the stress-strain curves decreased. At 15 °C/min treatment, the mineral composition and microstructural alteration in red granite may cause it to transition into an elastoplastic state. This is due to the differential thermal expansion of red granite minerals being uncoordinated, and microcracks are formed between the mineral particles, resulting in thermal strain. Hence,

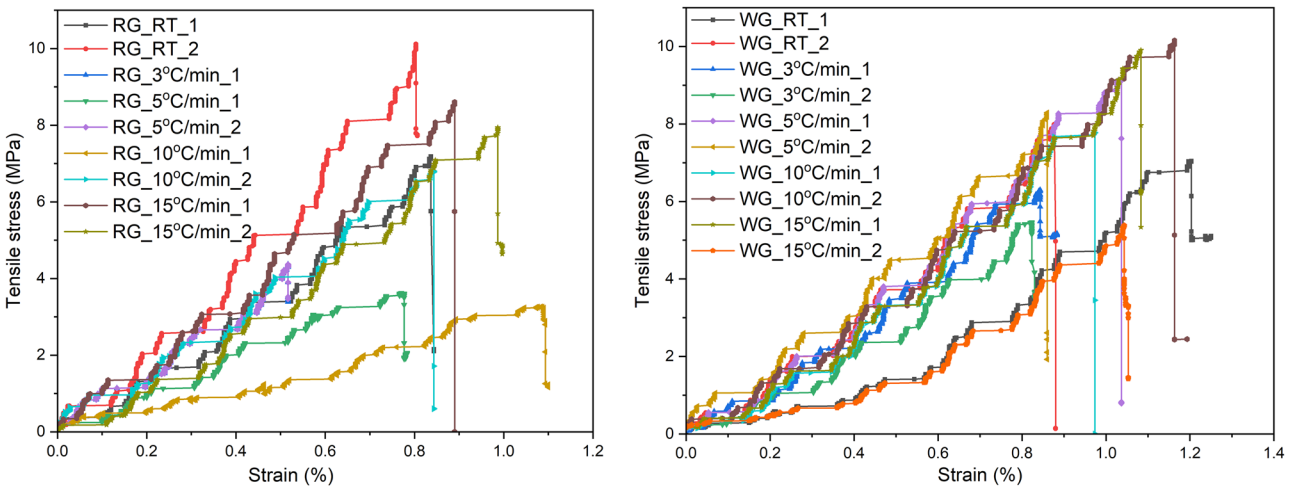

Fig. 8 Typical stress-strain curve under the tension after heat treatment. **a** Red granite. **b** White granite

post-failure curves exhibited a ductility characteristic after an increased heating rate in red granite. But, white granite has fewer thermally induced intergranular microcracks at a high heating rate > 10 °C/min. These microcracks progressively close under external force and during the loading stage, as a result in higher reversible deformation at the stage of crack damage.

Variation of strength and deformation

The variation of tensile strength and failure strain of granitoid at different heating treatments is shown in Fig. 9. The tensile strength of the red granite (RG) specimens decreased from the unheated condition by 49.15%, 53.76%, 41.69%, and 4.54% respectively at 3, 5, 10, and 15 °C/min heating rates. The increase in thermal cracks results in the difference in the local bearing capacity of red granite due to the change in the crack propagation stage. Above 10 °C/min heating rate treatment developed a thermal shock; the difference in the local bearing capacity of red granite increases, producing numerous local failures until it is destroyed. In contrast, the tensile strength of white granite is decreased by 22.59% at 3 °C/min heating rate. The decline in tensile strength of white granite caused by thermal damage is due to the development of cracks and the pre-existing thermally induced cracks. But, the tensile strength of white granite is increased by 14.91%, 18.29%, and 1.52% respectively at 5, 10, and 15 °C/min heating rates. The increase in strength can be explained by compaction in the specimen as the dilation of rock granules scrunches pre-existing fractures. Before the onset of new microcracks, the initial grain expansion closes the pre-existing microcracks, giving rise to a tighter structure. This is directly reflecting the reduction in porosity and densities too. After the crack closure, further grain expansion promotes the generation of microcracks due to the thermal expansion mismatch and anisotropy. Therefore, the dominancy of the strengthening effect upon different heating rates over weakening relies on the initial porosity

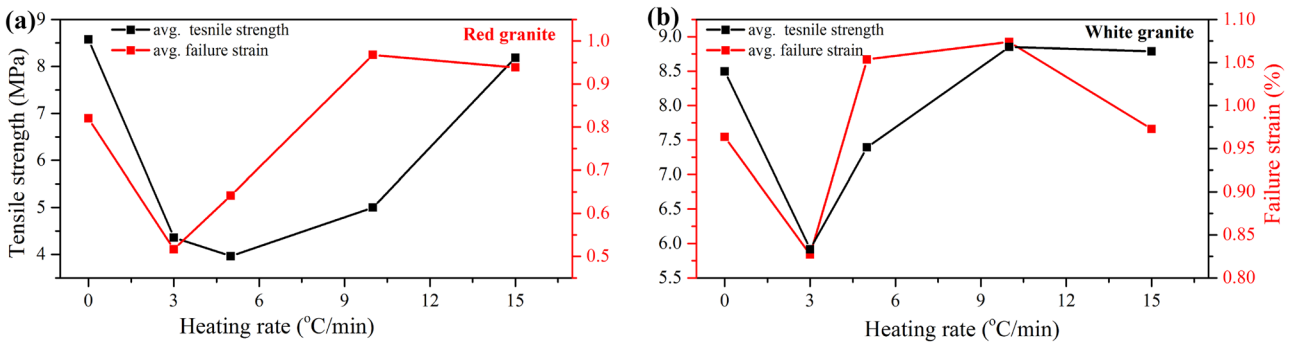

Fig. 9 Variation of strength and deformation. **a** Red granite. **b** White granite

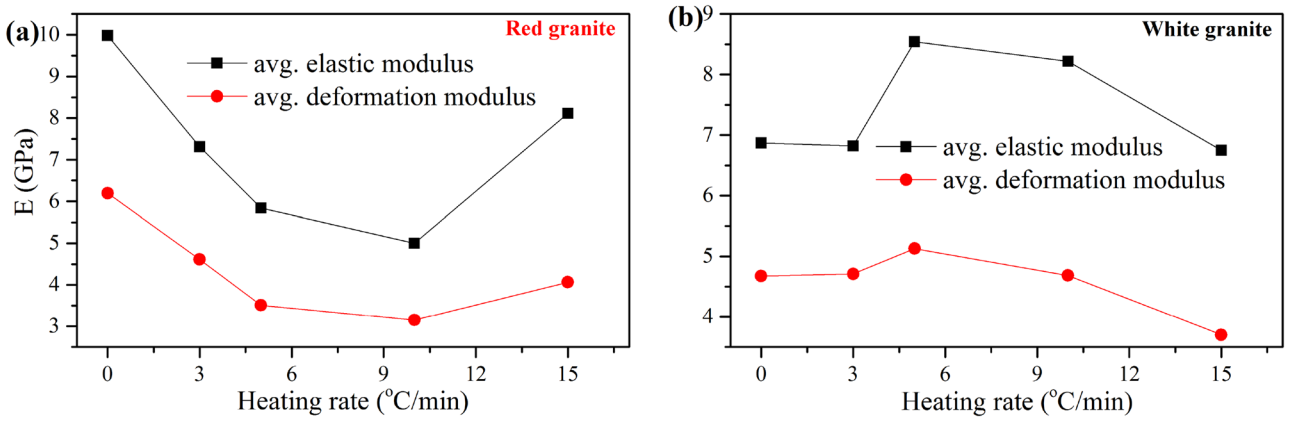

Fig. 10 Variation of elastic modulus and deformation modulus. **a** Red granite. **b** White granite

as well as the constitutive minerals. The main reason is the cohesion is weakening, while the friction is strengthened by increasing temperature from room temperature to 300 °C in different heating rate treatments in white granite.

Variation of elastic modulus and deformation modulus

The elastic modulus and deformation modulus of red granite as a function of the different heating rates are shown in Fig. 10a. The red granite elastic modulus and the deformation modulus decrease from unheated conditions by 26.75%, 41.48%, 49.94%, 18.68%, 25.57%, 43.36%, 49.14%, and 34.39% respectively at 3, 5, 10, and 15 °C/min. But after 3 °C/min heat treatment, the white granite elastic modulus decreases by 0.72%. In contrast, the elastic modulus is increased by 24.30% and 19.65% at 5 °C/min and 10 °C/min. But elastic modulus decreases by 1.74% at 15 °C/min during unheated conditions. The deformation modulus increases by 0.72%, 9.70%, and 0.18%, as compared to unheated conditions at 3, 5, and 10 °C/min. But, after 15 °C/min heating rate treatment deformation modulus decreases by 20.82% from the unheated conditions as shown in Fig. 10b. The inconsistency between the elastic modulus and the deformation modulus reflects the reversible elastic deformation and irreversible elastoplastic deformation. The elastic modulus is caused by the anisotropy of thermal expansion within different minerals, while the deformation modulus is caused by thermal gradient–induced cracks that can form when thermal stresses are caused by an inhomogeneous temperature field that exceeds the rock's local tensile or shear strength. The increase in irreversible plastic deformation in red granite was mostly induced by the treatment when the heating rate is above 5 °C/min. As a result, coarse-grained red granite is more prone to elastoplastic transition than fine-grained white granite (Gautam et al. 2019a, 2020).

Thermal damage evolution

Mechanical deterioration of the rock is primarily induced by the initiation, propagation, and coalescence of cracks in rocks. The failure process of brittle rock has been described using two kinds of damage models: microscopic and macroscopic. Although the rock is considered to be a homogeneous material in continuum damage mechanics, the failure process is attributed to a decrease in elastic modulus as a result of internal damage. This model was developed theoretically and is rigorously founded on science and evidence (Krajcinovic and Silva 1982; Chang et al. 2022). The other damage model suggests that the damage variable is a distribution, and the damage is investigated using the microscopic statistical damage theory. Damage to the rock occurs in two stages. The first is microscopic (damage resulting from microcracks in the rock material) and the second is macroscopic (damage factor as a result of the accumulation of failures in the mesoscopic components). Since microcracks and micro-voids in rock materials are randomly distributed, and rock strength is assumed to obey the Weibull statistical distribution, which is described in Eq. (2):

$$f(\varepsilon) = \frac{m}{F}\left(\frac{\varepsilon}{F}\right)^{m-1} \exp\left[-\left(\frac{\varepsilon}{F}\right)^{m}\right] \tag{2}$$

where $f(\varepsilon)$ is the distribution function of the strength of rock microelements, ε is the random distribution variable of the microelement strength, and m and F are the Weibull distribution parameters. According to the strain elastic theory of rock, the original microcracks inside the rock develop and evolve, resulting in continuing damage to the rock; hence, the microscopic damage variable (D) can be defined as Eq. (3):

$$D = \frac{V_P}{V} = \frac{\iiint_V \int_0^{\varepsilon} f(\epsilon) d\varepsilon \, dx \, dy \, dz}{V} \tag{3}$$

where V is the total volume and V_P is the damaged volume rock. When Eq. (1) is substituted for Eq. (2), the damage variable is described as follows:

$$D = 1 - \exp\left[\left(\frac{\varepsilon}{F}\right)^m\right] \tag{4}$$

Thus, the stress-strain relationship is

$$\sigma = E_o \varepsilon (1 - D) \tag{5}$$

where D is the microscopic damage, and E_o is the elastic moduli of the intact rock.

However, to calculate the two m and F variables, the used technique in this study was suggested by Wu and Zhang (1996).

$$F = \frac{\varepsilon_P}{\left(\frac{1}{m}\right)^{1/m}} \tag{6}$$

$$m = \frac{1}{\ln\left(\frac{E_o \varepsilon_p}{\sigma_p}\right)} = \frac{1}{\ln E_o - \ln E_d} \tag{7}$$

where σ_p is the peak stress, and ε_p is the corresponding failure strain at the peak stress. E_d and E_o are deformation modulus and elastic modulus which can be determined by the stress-strain curve from the test. Thus, microscopic damage can be calculated from Eqs. (2) to (7):

$$D = 1 - exp^{\left(\frac{\varepsilon}{F}\right)^m} \tag{8}$$

Equation (5) can be rewritten as

$$\sigma = E_o \varepsilon e^{-\frac{1}{m}\left(\frac{\varepsilon}{\varepsilon_p}\right)^m} \tag{9}$$

If the macroscopic damage is considered, the stress-strain relationship described in Eq. (5) can be written as:

$$\sigma = E_T \varepsilon (1 - df) \tag{10}$$

where the df is the damage factor and $E_T = E_o(1 - df)$ is the new elastic modulus of thermally treated materials. As a result, the thermal damage factor (df) may be calculated as follows in Eq. (11):

$$df = 1 - \frac{E_T}{E_O} \tag{11}$$

It is found that as the heating rate increases, the microscopic damage increases by 0.58, 0.81, 0.92, and 0.93, respectively, for red granite as shown in Fig. 11a. This is maybe due to the mineral grain expansion which causes the corresponding change in the rock volume under heat treatment. The localized thermal stress will be produced within or among the grains due to the differential thermal expansion of minerals. In contrast, restraining and expansion will result in grains with high and low expansion rates, respectively. Thus, the original structural pattern of rock will be demolished, causing the formation of a new one and propagation of pre-existing microcracks. Then, the stress of the rock material exceeds the yield point, and the plastic deformation occurs. Hence, the new microcracks begin to expand between the relatively weak grain boundaries, and the rock damage begins to evolve and unstably expand. With increased stress, thermal cracks inside the rock become densely concentrated and connected forming macroscopic damage. At last, the macroscopic cracks are connected to form the main rupture surface, which leads to the sudden release of the stress. The rock strength decreases rapidly, and the damage tends to 1. The microscopic damage increased to 0.87, 0.77, 0.63, and 0.89, respectively, for white granite as shown in Fig. 11b. The reason is that the axial load improves the rock's stress state and restrains and enhances

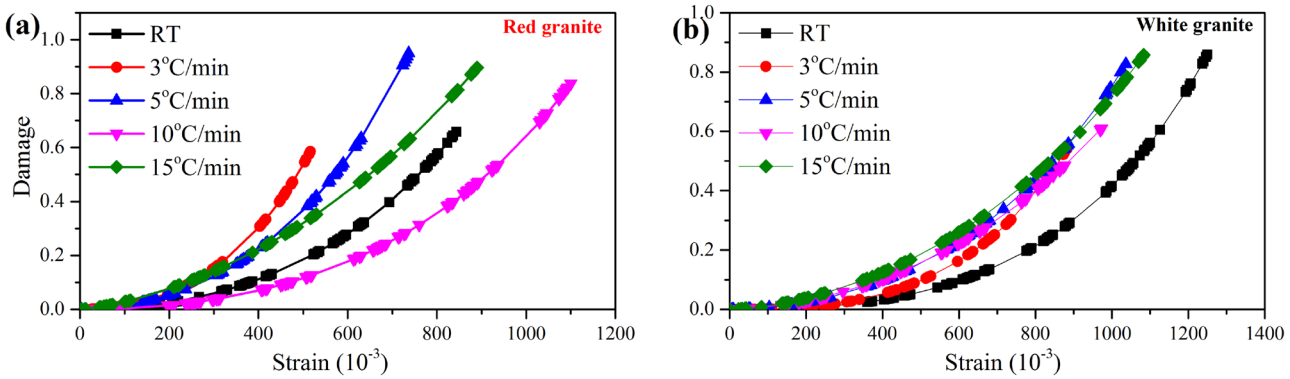

Fig. 11 Thermal damage evolution under different heating rates. **a** Red granite. **b** White granite

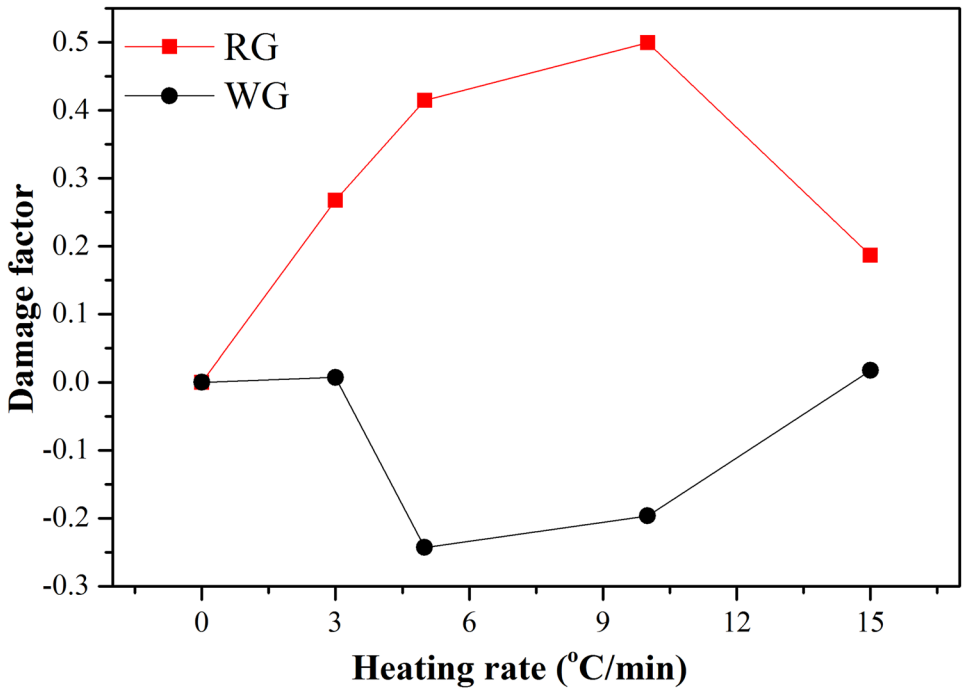

Fig. 12 Variation of damage factor

its macroscopic damage average intensity. But the slope of the damage curve decreases with the increase of strain. This indicates that the stress increases the dislocation of the rock particles, weakens the strain recovery ability, and enhances rock brittle-ductile failure. On the other hand, results of macroscopic damages after 3, 5, 10, and 15 °C/min heating rate treatment of red and white granite are shown in Fig. 12. The damage factor of the red granite (RG) is constantly increased by 0.26, 0.41, and 0.49. But some decrease by 0.18 after 15 °C/min heating rate treatment. In contrast, the damage factor in white granite (WG) is constantly decreased by 0.007, 0.24, 0.19, and 0.017. The variances of damage factors of RG and WG granitic rocks depend on the number of microdefects (pre-existing cracks and microfractures). This directly reflects the damage factor of granite caused by increasing heating rate treatment. As a result, increasing heating rates lead to more microscopic cracks in the red granite as compared to white granite. These microscopic cracks increase the voids of the red granite (RG), which leads to an increase in the damage factor. The mineralogical compositions of granite are quartz, albite, plagioclase feldspar, and biotite which have not changed when the maximum temperature of granite is 450 °C (Xi 1994; Shang et al. 2019; Pai et al. 2021), therefore resulting in an increase of the air content in the microvoids of red granite (RG), as well as the increase of contact thermal resistance between white granite (WG) mineral particles. This is the main contributor to the increase in the damage factor of red granite. However, contact thermal resistance is a resistance-like term used to describe the resistance to heat transfer. There are two components to the contact thermal resistance between rock mineral grains. One is the thermal resistance generated by the actual contact area of grains, and the other is the thermal resistance generated by the microvoids (Incroera et al. 2007). The number of microvoids between red granite (RG) mineral particles has increased significantly as compared to white granite (WG) between 10 and 15 °C/min heating rate. This is due to the number of microvoids between mineral grains in red granite having risen, resulting in a change in the heat conduction mechanism from the actual contact grain area through the microvoids.

Variation of brittleness

Brittleness is a material's ability to deform elastically without apparent permanent deformation whenever the stress distribution exceeds the crack-initiation stress threshold. However, there is no universally accepted classification for rock brittleness. For instance, in the previous investigation, several criteria have been introduced to classify the brittleness (based on strength parameter, mineral compositions, and stress-strain curve) of rock materials. It is widely accepted that a brittleness index based on stress-strain curves

of rock brittleness is the most regularly applied in rock mechanics. Additional investigation was conducted into the strain sensitivity of the mobilized strength and the entire failure process (pre- to post-peak stages) to the strength components for cohesion weakening and frictional strengthening. The brittleness cohesion loss and frictional hardening rates are anticipated as damaged plastic strain (ε_c^p and ε_f^p) to be influenced by the rock mass and loading characteristics. The strain-dependent brittleness index concept was used for mobilization of strength which explicitly addresses the contribution of the cohesive and frictional strength components during the entire failure process using the following equation (Eq. (12)).

$$BI_{\varepsilon} = \frac{\varepsilon_f^p - \varepsilon_c^p}{\varepsilon_c^p} \tag{12}$$

Here, ε_f^p is the frictional plastic strain and ε_c^p is the cohesive plastic strain.

The stability in the granitoid (red and white granites) can be related to differences in their brittleness after heating treatment as shown in Fig. 13. The red granite has greater heterogeneity and anisotropy of mineral composition and its grain size contributes to a slower cohesion loss rate (with straining) and/or faster frictional strengthening (fast friction hardening, that is, higher brittleness). This may be due to the mismatch of thermal expansion coefficients between adjacent minerals which leads to grain boundary cracking. In contrast, in white granite the intergranular flaw size plays the role of strongly linked in initiating the microcracks that occur within a grain due to the differential thermal expansion of the mineral. This might be used to argue that, in fine-grained crystalline rocks, the intergranular cracks are more abundant than in coarse-grained rocks. The propagation of intergranular cracks (there are more fine-grained rocks) mobilizes more strength, owing to the increased involvement of frictional strength and/or the slower cohesion loss. The propagation of intergranular cracks is more brittle and involves a lower frictional strength contribution. This leads to the conclusion that homogeneous fine-grained white granite tends to possess lower brittleness than heterogeneous coarse-grain-sized red granite rocks. The stability in the granitoid (RG and WG) can be related to differences in their brittleness.

Failure morphology

The failure morphology after heating treatment can well reflect the damage level of the internal rock structure in red and white granite as shown in Fig. 14. The red and white granitic rock's structure was dense at room temperature, and its failure was mostly due to the tensile fractures in both rocks. However, microcracks were formed in the

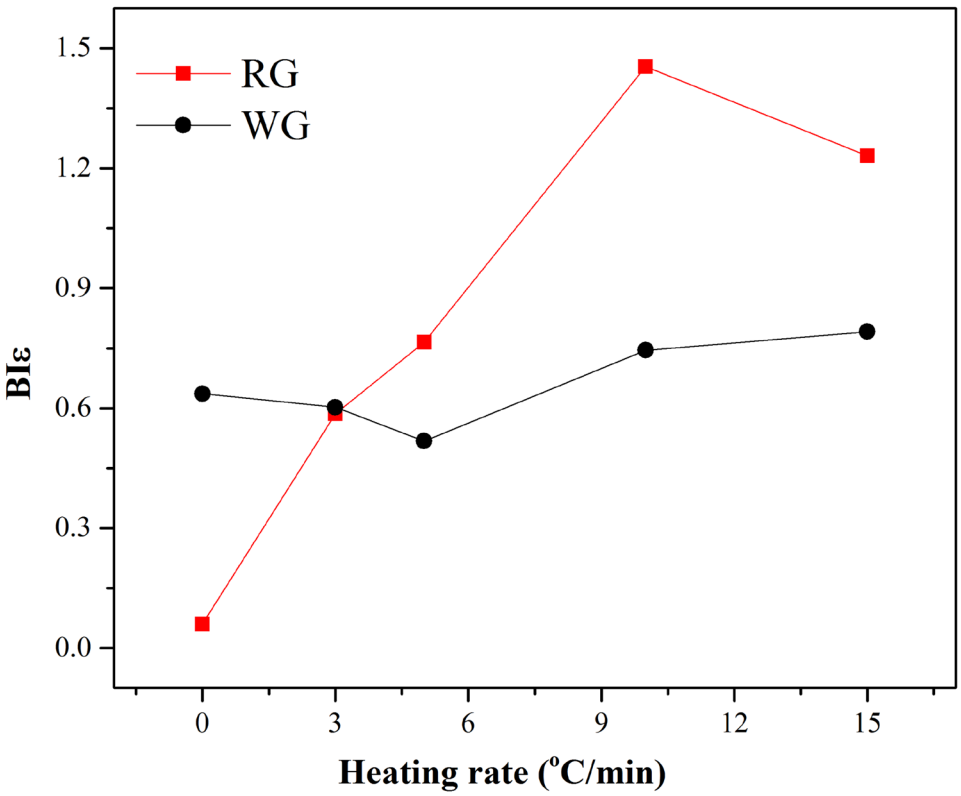

Fig. 13 Variation of brittleness

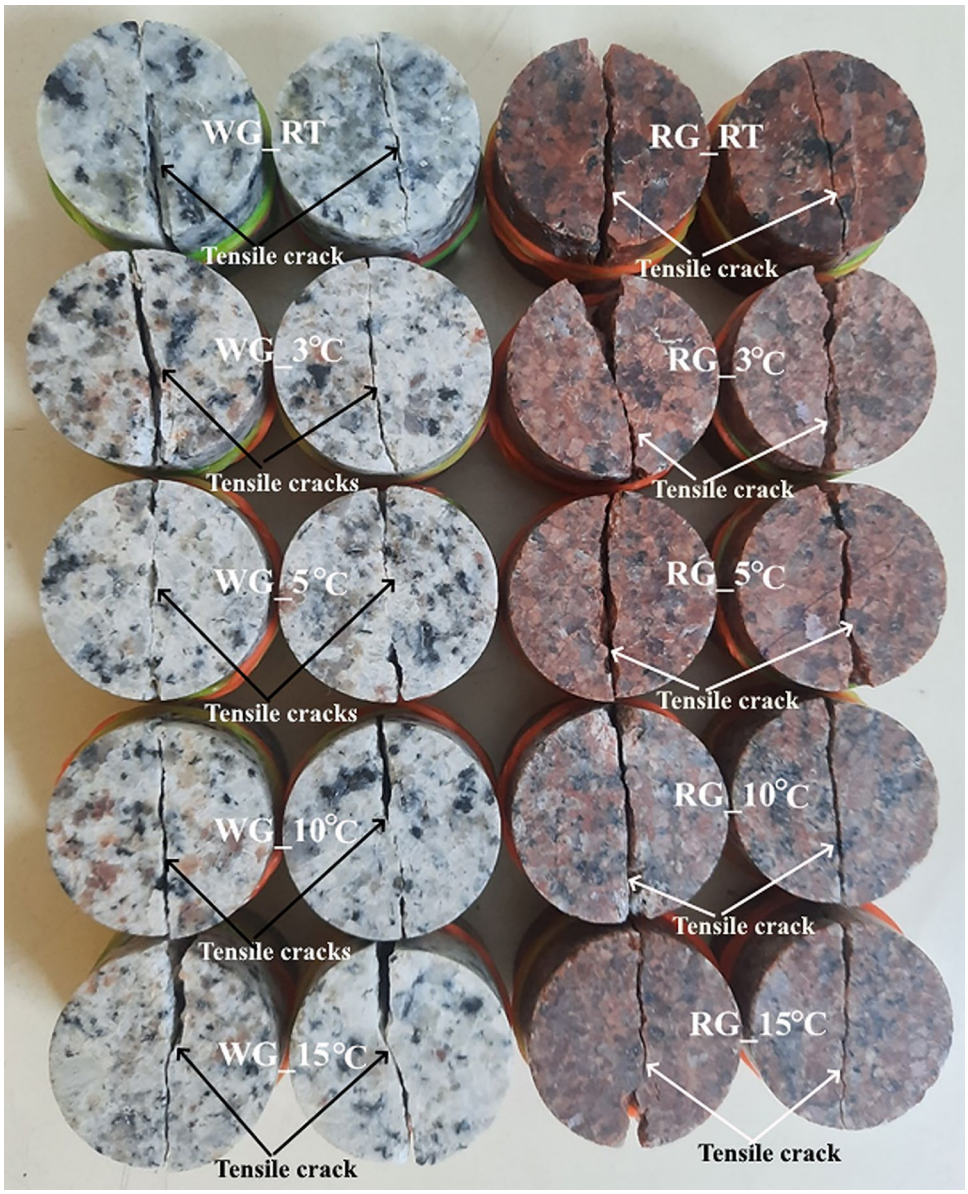

Fig. 14 Macroscopic failure morphology of red and white

granite after the 3 and 5 °C/min treatments. The microcracks interconnected to form many weaker planar structures under the influence of axial stress. The development of which was enhanced by the increasing axial stress. Hence, in white granite, weak plane structures approximately parallel to the loading direction formed preferentially. This prevents the growth of other weak plane structures and eventually results in tensile failure. While, in red granite, the weak plane structures that are 83° to 87° angled about the loading direction also exceeded their tensile strength, resulting in the formation of tensile fractures. The main reason for this is in white granite when the heating rate increases, initial grain expansion closes pre-existing microcracks, resulting in a more compact structure after axial loading. But in red granite, the differential thermal expansion along the mineral grain boundaries has formed thermally induced microcracks. Hence, the heating rates increased, and local spalling failure occurred. This revealed that both the red and white granite form many weak plane structures, but also locally deteriorated damaged zones. These deteriorated zones were triggered by axial force, resulting in the formation of local spalling zones. Thus, tensile failure prevailed in the red and white granite at the 15 °C/min treatment. The main effect of microcracking on rock strength involves two possible mechanisms, based on whether thermally induced microcracks play a dominating role and whether thermally induced and stress-induced microcracks interplay.

Variation of thermal expansion and thermal strain

The host rock in the NWR will expand due to transient thermal response. Therefore, understanding thermal expansion and thermal strain is essential. The thermal expansion and thermal strain of coarse and fine mineral grains were changed to observe the effect of heterogeneity and anisotropy on the thermal damage process. However, thermal expansion is generally understood to be caused by the influence of anharmonic factors in the potential energy on the mean separation of atoms at a given temperature. Thermal expansion is proportional to the potential energy of the mineral particles. Moreover, the lattice structures and regular periodic elements or cluster arrangements constitute the crystal structure of the rock. The potential energy of the mineral particles (such as atoms) in the lattice is determined by the bonding force between the grains. The higher the potential wall of particles, the stronger the bonding force between the mineral particles becomes. The smaller the thermal expansion coefficient, the less the particle amplitude increases when the temperature rises to the same level. Thus, anharmonic components in potential energy have long been recognized to induce thermal expansion, which is why mineral particles tend to separate farther at a higher heating rate. Then, this relationship between thermal expansion and the potential energy of mineral particles (like atoms) in the lattice is based on the bonding force between the grains. Therefore, the bonding force between molecules in fine-grained white granite crystals is often lower than in coarse-grained red granite crystals. The thermal expansion of red granite is 10.94 × 10-6 K^{-1}, 11.16 × 10-6 K^{-1}, 11.48 × 10-6 K^{-1}, and 12.63 × 10-6 K^{-1} during 3, 5, 10, and 15 °C/min respectively as shown

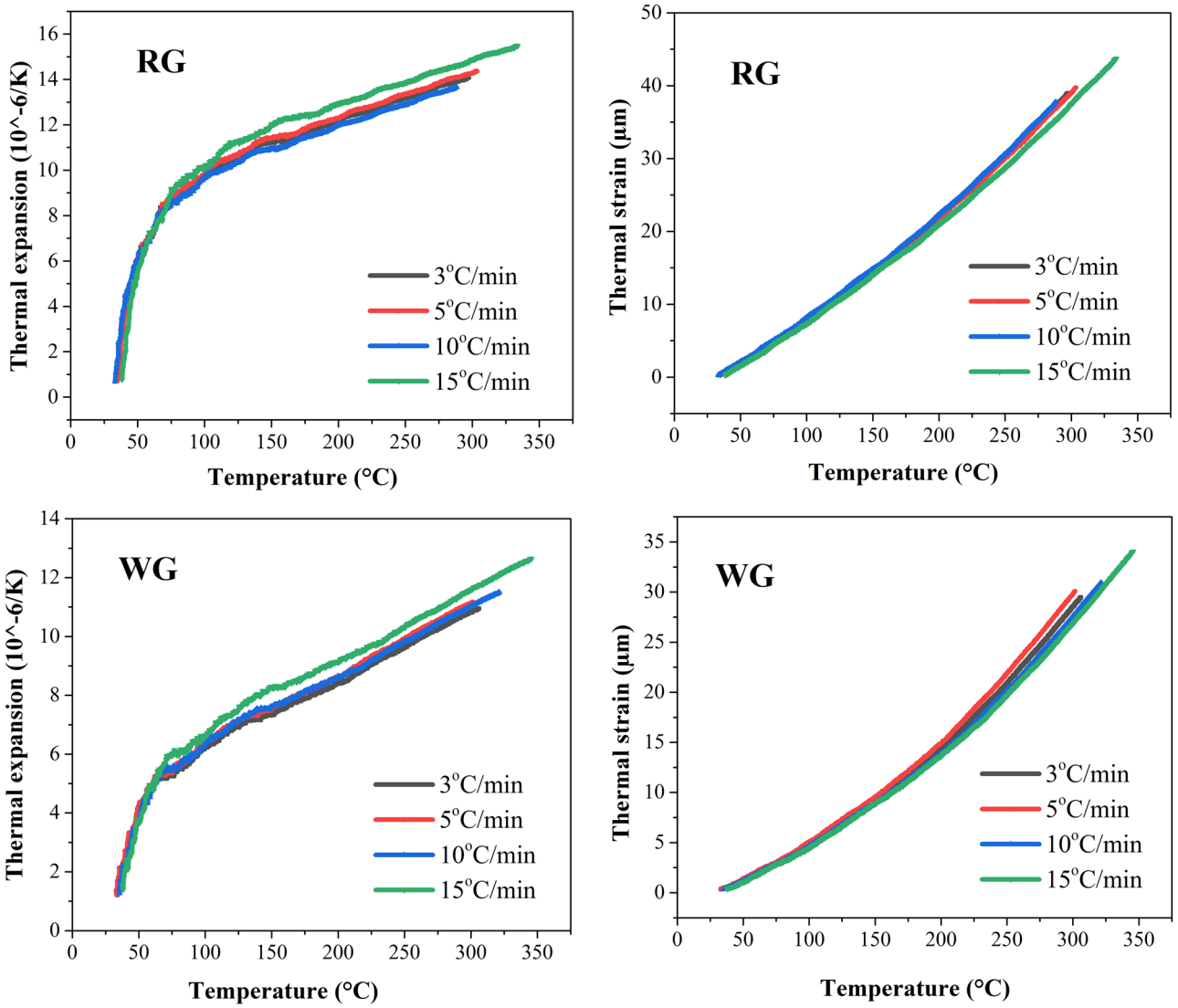

Fig. 15 Thermal expansion and thermal strain of red and white granite

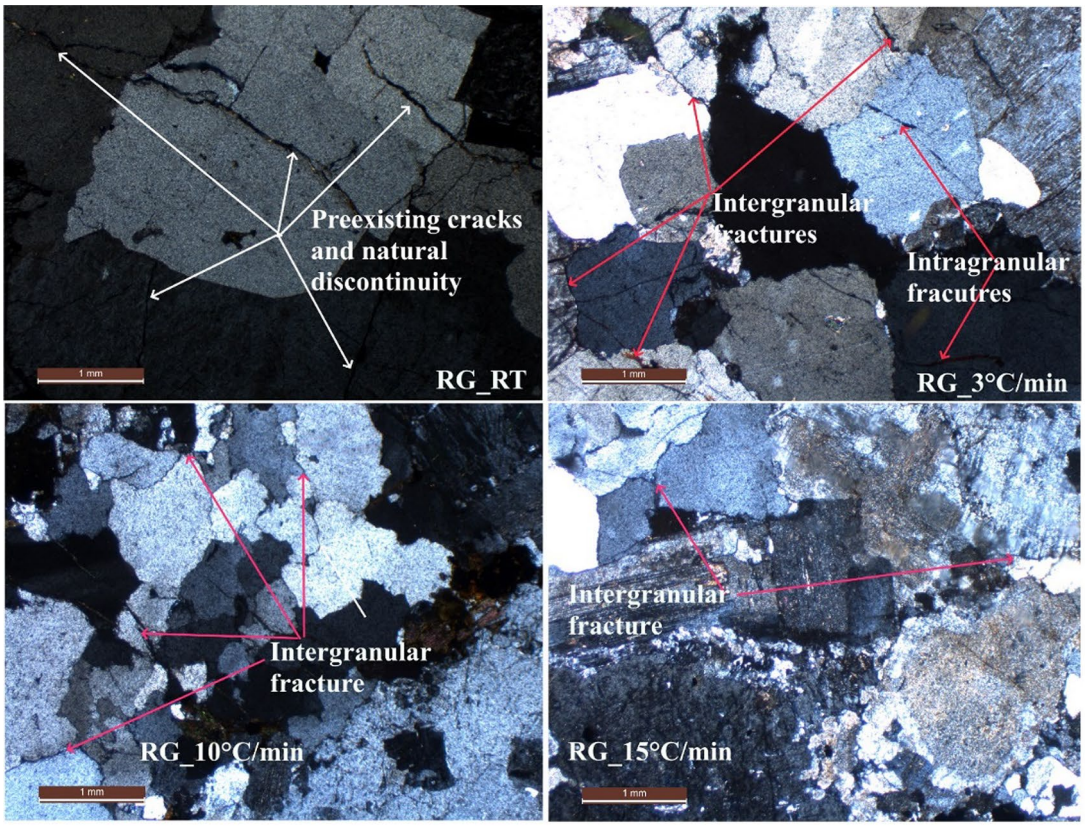

(a)

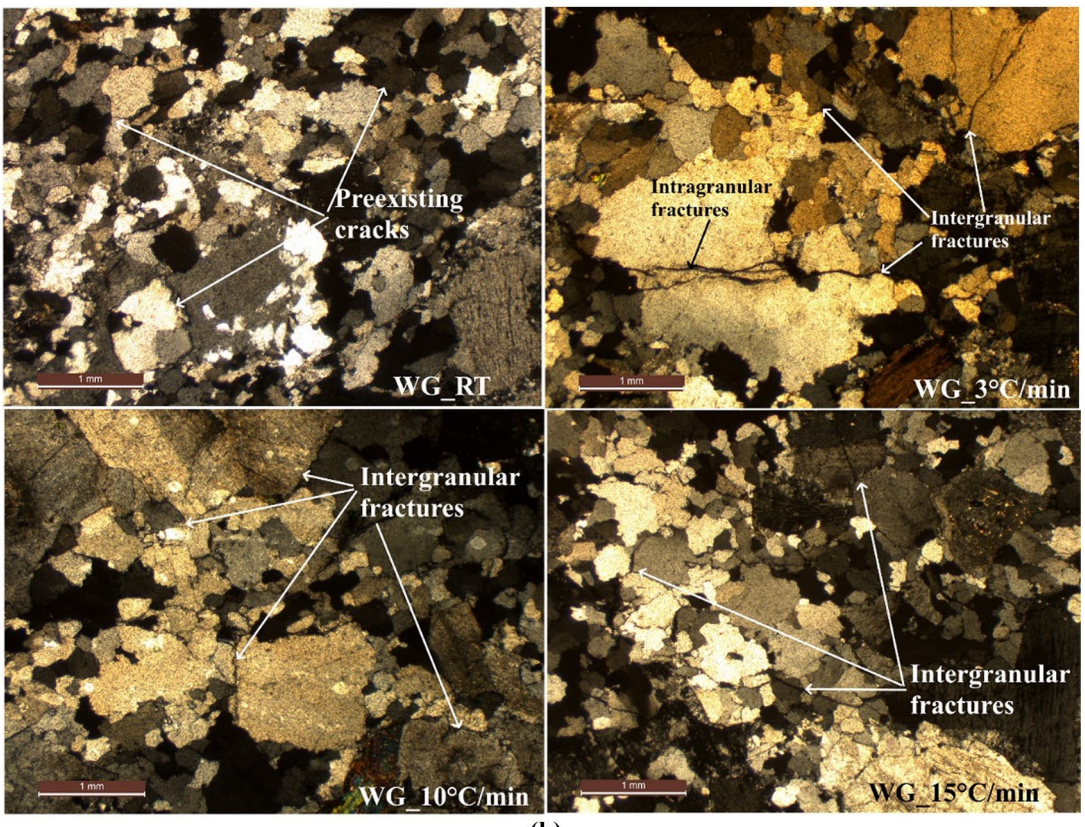

(b)

Fig. 16 Microscopic observation. **a** Red granite. **b** White granite

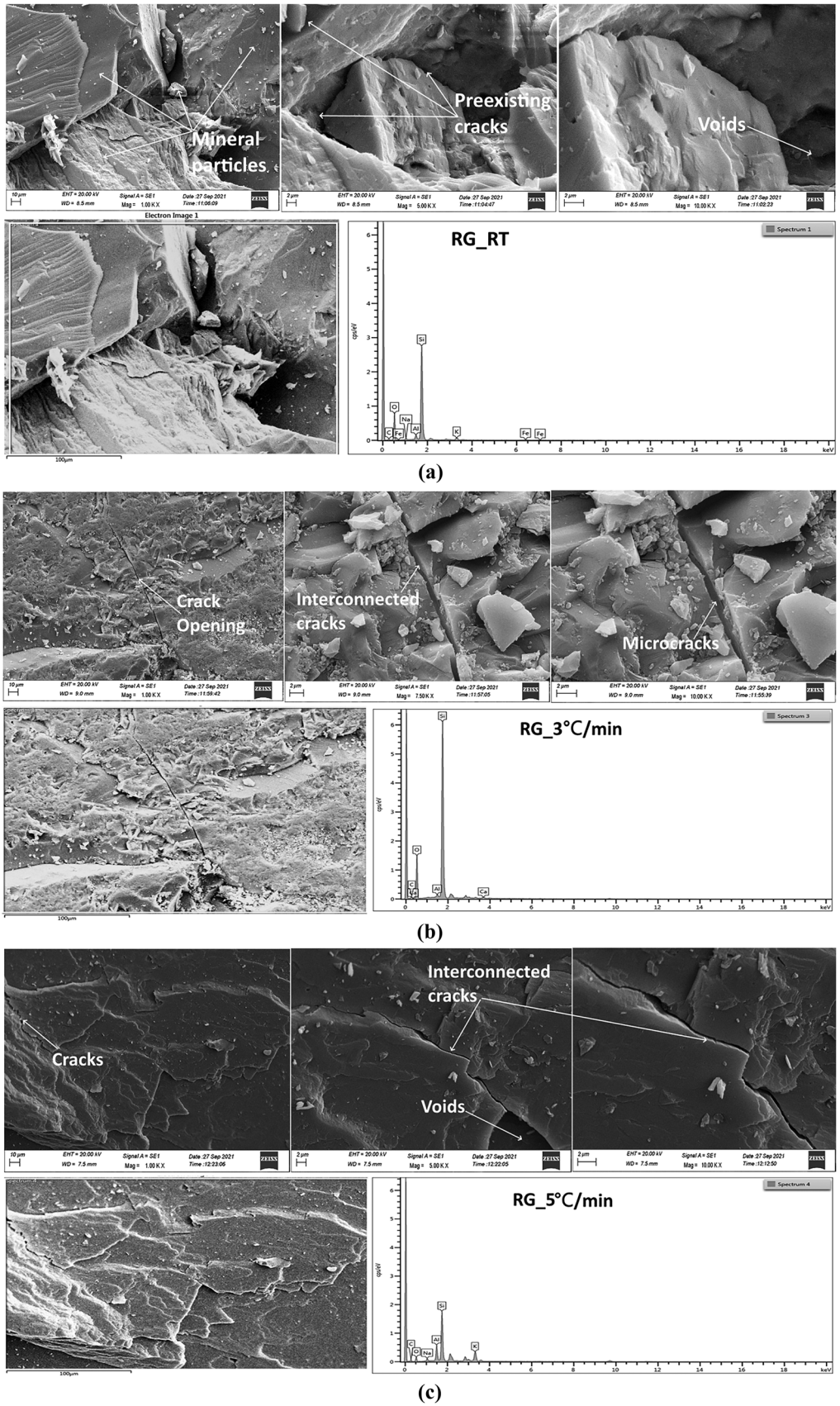

Fig. 17 SEM analysis of red granite. **a** RT. **b** 3 °C/min. **c** 5 °C/min. **d** 10 °C/min, and **e** 15 °C/min

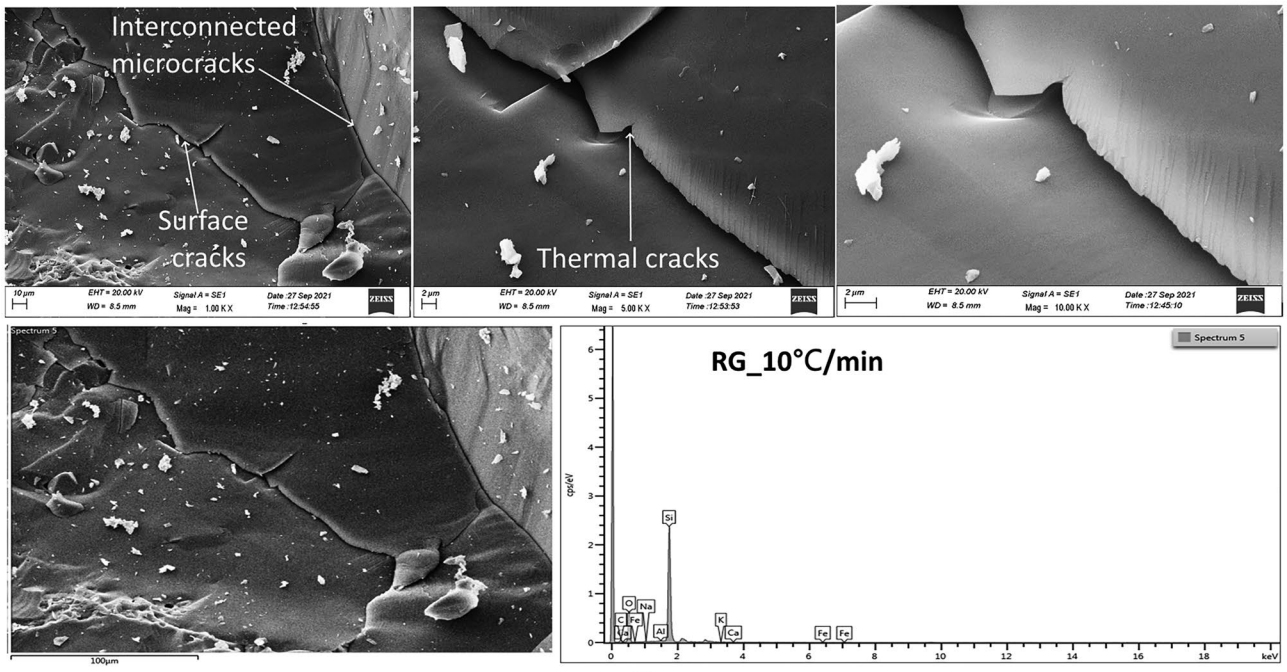

Fig. 17 (continued)

in Fig. 15. The coarse grain–based rocks have a heterogeneous thermal expansion that is extensive enough to allow concentrated stresses to develop within the specimens, producing inter-granular tensile microcracking due to thermal expansion anisotropy. In contrast, the thermal expansion of white granite is 13.64 × 10-6 K^{-1}, 14.07 × 10-6 K^{-1}, 14.36 × 10-6 K^{-1}, and 15.48 × 10-6 K^{-1} at 3, 5, 10, and 15 °C/min respectively. This is due to the thermal expansion anisotropy within individual grains. When thermal stress exceeds the tensile strength between mineral grains, intragranular cracking occurs. Thus, quartz has the highest thermal expansion coefficient among other common rock-forming minerals (e.g., k-feldspar, plagioclase, and biotite mica) (Gautam et al. 2019b). The volume expansion of quartz is about four

times that of feldspar. The comparison of fine-grained white granite to coarse-grained red granite contains a greater variety of mineral components and larger crystal particles with a high thermal expansion coefficient, which increases the interface area between the various mineral particles and results in the coarse-grained granite's extreme heterogeneity. As a result of its great heterogeneity and larger grain size, coarse-grained red granite produces more concentrated and higher thermal stress over a wider range when subjected to a high heating rate. Hence, coarse-grained red granite is more prone to developing a large-scale thermally induced crack, resulting in a lower thermal expansion. The thermal strain vs temperature curves are non-linear for the red granite, and when the temperature increases from 35 to 300 ℃, the thermal strain increase to 29.46, 30.05, 30.93 and 34.02 (in μm) at 3, 5, 10, and 15 ℃/min, respectively. This thermal strain

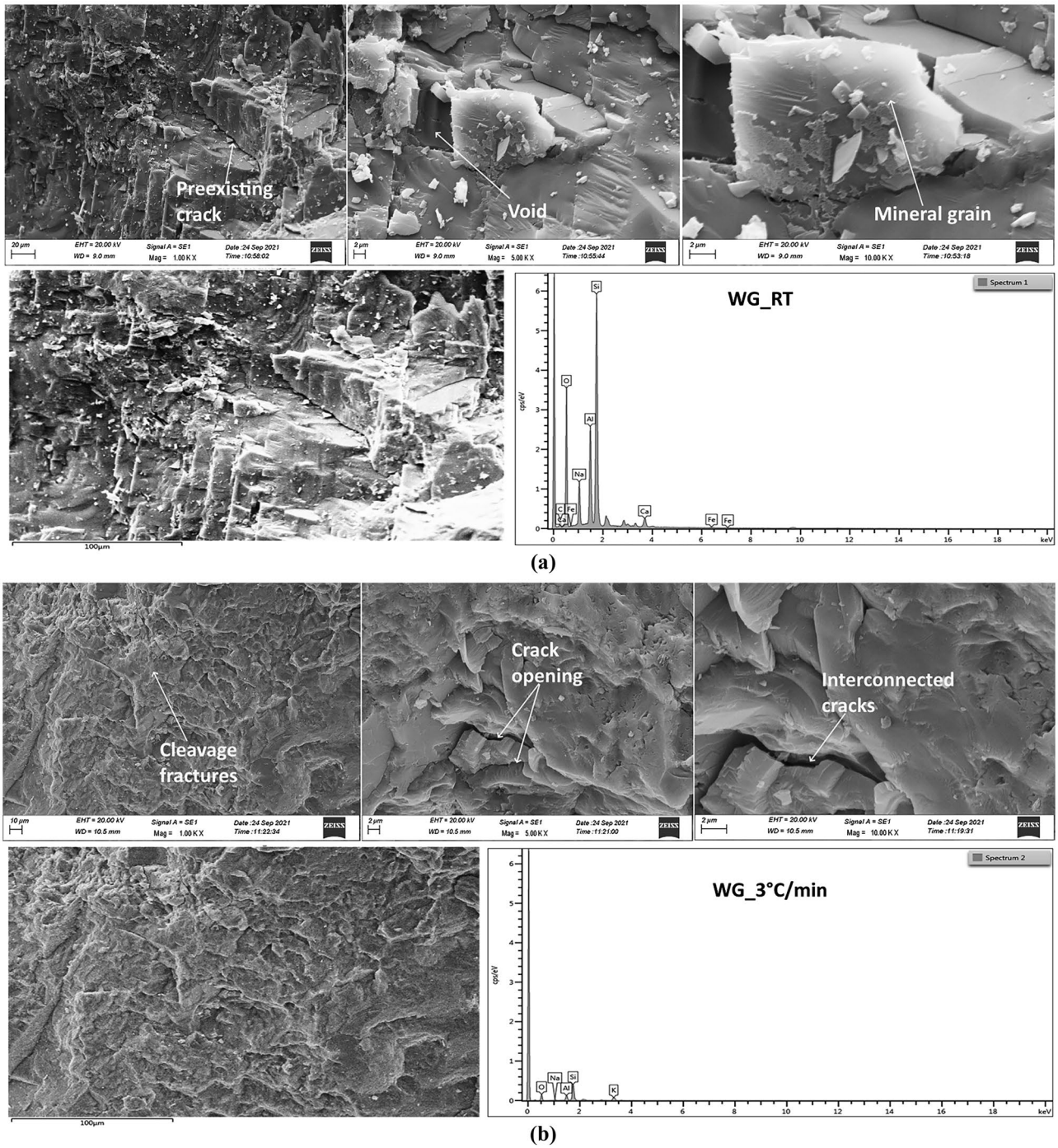

Fig. 18 SEM analysis of white granite a RT **b** 3 °C/min **c** 5 °C/min **d** 10 °C/min and **e** 15 °C/min

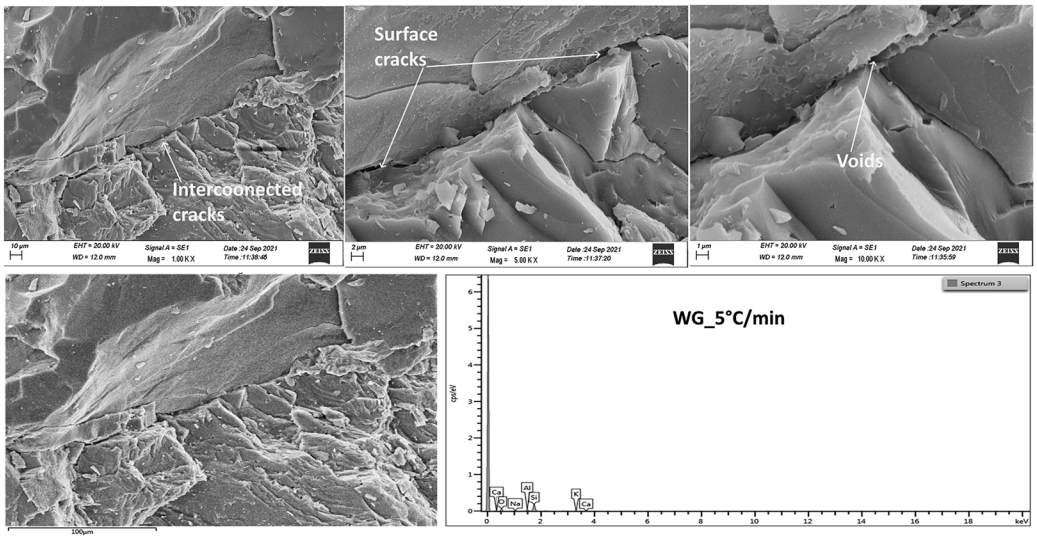

(c)

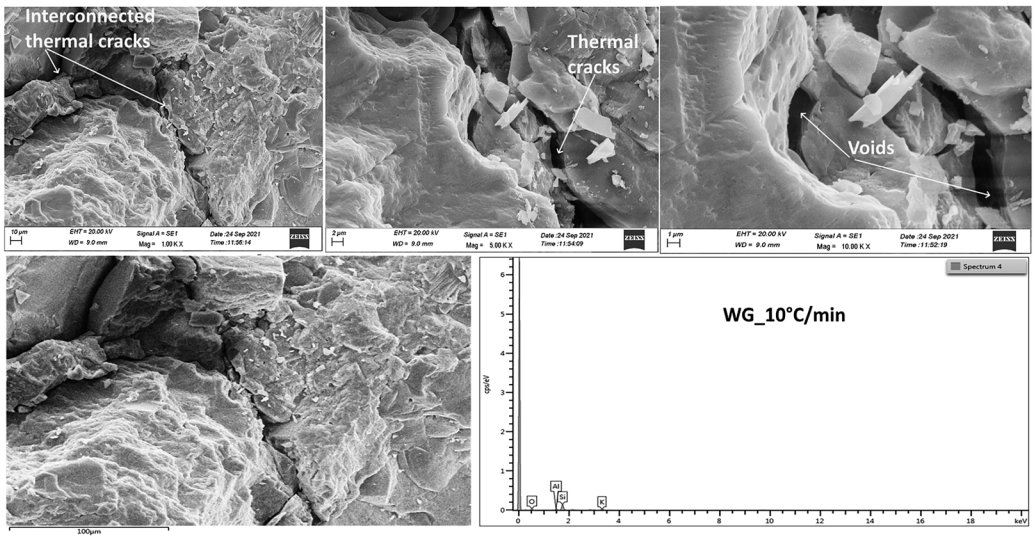

(d)

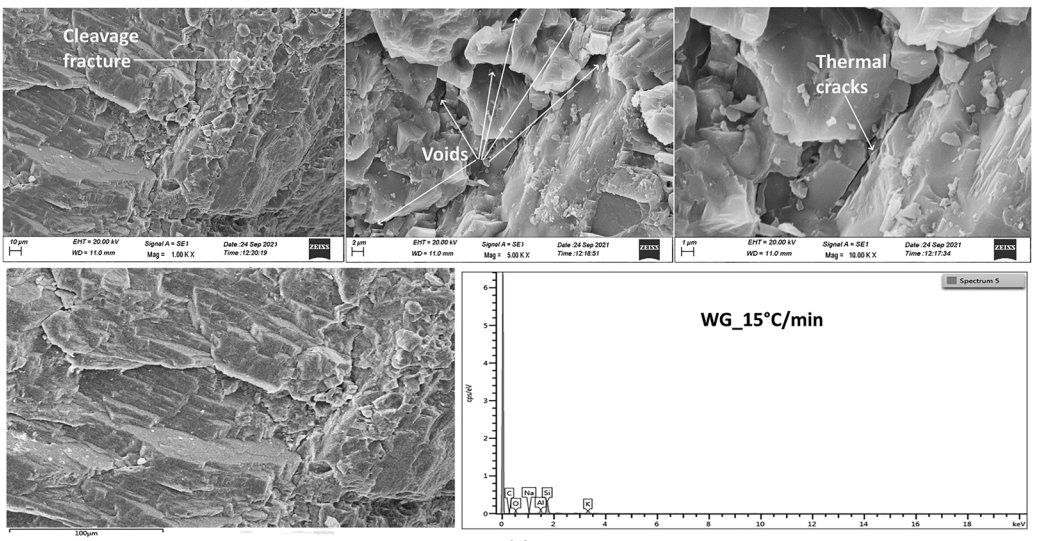

(e)

Fig. 18 (continued)

variation cannot be verified because the change is too small to be detected experimentally with our dilatometer. While, in white granite, the thermal strain curves increases linearly by 38.93, 39.73, 37.74, and 47.70 (in μm) at 3, 5, 10, and 15 °C/min, respectively. It was observed that the effect of heating causes differential thermal expansion of mineral grains making up the rocks which may lead to intergranular fracturing, thus increasing the porosity of the heated rock.

Microscopy observation

If the temperature field is uniform, two mechanisms produce the localized tensile stress in granites: thermal expansion coefficient mismatches between different minerals and thermal expansion anisotropy within an individual mineral (Zhao et al. 2018). Generally, thermal microcracking behavior against temperature treatment proceeds as follows: a slight reduction in the aperture of existing microcracks; a significant closure of existing microcracks; a marginal progressive widening of existing microcracks; the beginnings of new grain boundary cracks; the progressive development of new grain boundary cracks; acceleration of intergranular cracking together with intragranular cracking and almost complete separation of all the grains. Thermal cracks can occur in both the intergranular and intragranular microcracks. The optical microscopy investigation revealed evidence of thermal cracking. In the temperature range of 20 to 300 °C, chemical reactions become inactive, and as a result, according to the generalization previously, thermal damage does not occur (Zhao et al. 2018; Wang and Konietzky 2019). For instance, rock-forming minerals require heat treatment at high temperatures, such as the transformation of quartz at 573 °C, the decomposition of clay minerals at 400–700 °C, and the decomposition of carbonite minerals at 700–830 °C, and feldspar and micas show little or no change even at 900 °C (Hajpál 2002).

The thin section photos of unheated and heated coarse-grained red granite and fine-grained white granite samples are shown in Fig. 16. The basal cleavage in coarse-grained red granite is more visible in the heated sample than in the unheated specimen because the expansion along granular boundaries opened the mica grains. Intragranular and intergranular cracks may have occurred during heating or may have developed as a result of pre-existing cracks expanding. In contrast, the initial grain expansion closes pre-existing microcracks, resulting in fine-grained white granite's tighter structure before the onset of new microcracks. As a result of heating treatment, grain expansion is seen as the only response. For this, rock structures have been identified as the primary source of strength improvement. This may have been due to new intragranular cracks occurring within some of the quartz crystals. Although, fined grain granite exhibits longer and more open intergranular cracks than more coarse grain granites. Hence, the coarse-grained red granite has a significant number of pre-existing cracks at room temperature, compared to the compacted, non-fractured fine-grained white granite (Ersoy et al. 2019). At above 5 °C/min heating rate treatment, due to the differential thermal expansion, cracking can still propagate and interconnect each other to form more developed thermal cracks than that of the fine-grained granite. This indicates that the coarse-grained granite experiences more intense and concentrated thermal cracking. It can be concluded that the average size of the major mineral in coarse-grained red granite, such as k-feldspar and plagioclase, is larger than that of the major mineral in fine-grained white granite, such as feldspar and quartz, with a maximum difference of 12 times. This leads to a larger interface area between the different mineral particles and the crystal particle size of coarse-grained granite is significantly larger than that of fine-grained granite from a macroscopic perspective (Yin et al. 2021).

SEM–EDX analysis

Thermal damage to the granitoid microstructure has an influence on its mechanical properties and increases the porosity. According to the microstructure observation, temperature changes can lead to microcrack formation, which is usually known as thermally induced microcracks,

Table 2 Variation of elemental compositions

Heating rate (°C/min)	C	O	Al	Si	Ca	Na	K	Fe
WG_RT	10.55	44.51	10.36	26.26	1.72	6.36		0.24
3		44.27	9.89	32.95		2.22	10.67	
5		45.94	6.11	41.85	1.03	3.84	1.23	
10		40.31	6.33	42.54			10.82	
15	18.02	33.97	8.26	27.57		2.07	10.11	
RG_RT	11.23	42.97	1.67	40.71		0.65	1.78	1
3	12.55	42.27	0.59	44.05	0.54			
5	22.87	18.52	9.5	34.5		2.16	12.44	
10	12.75	43.74	0.12	43.01				0.38
15	18.18	38.22		42.78	0.07	0.2	0.43	0.13

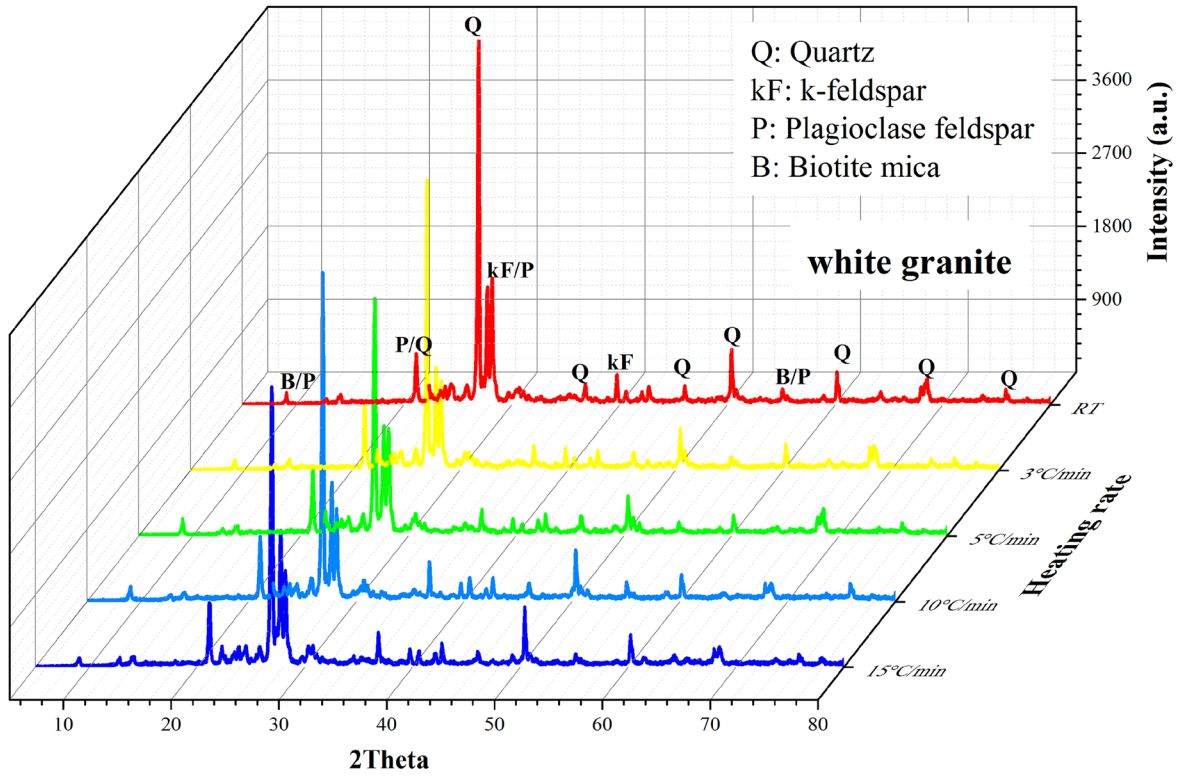

(a)

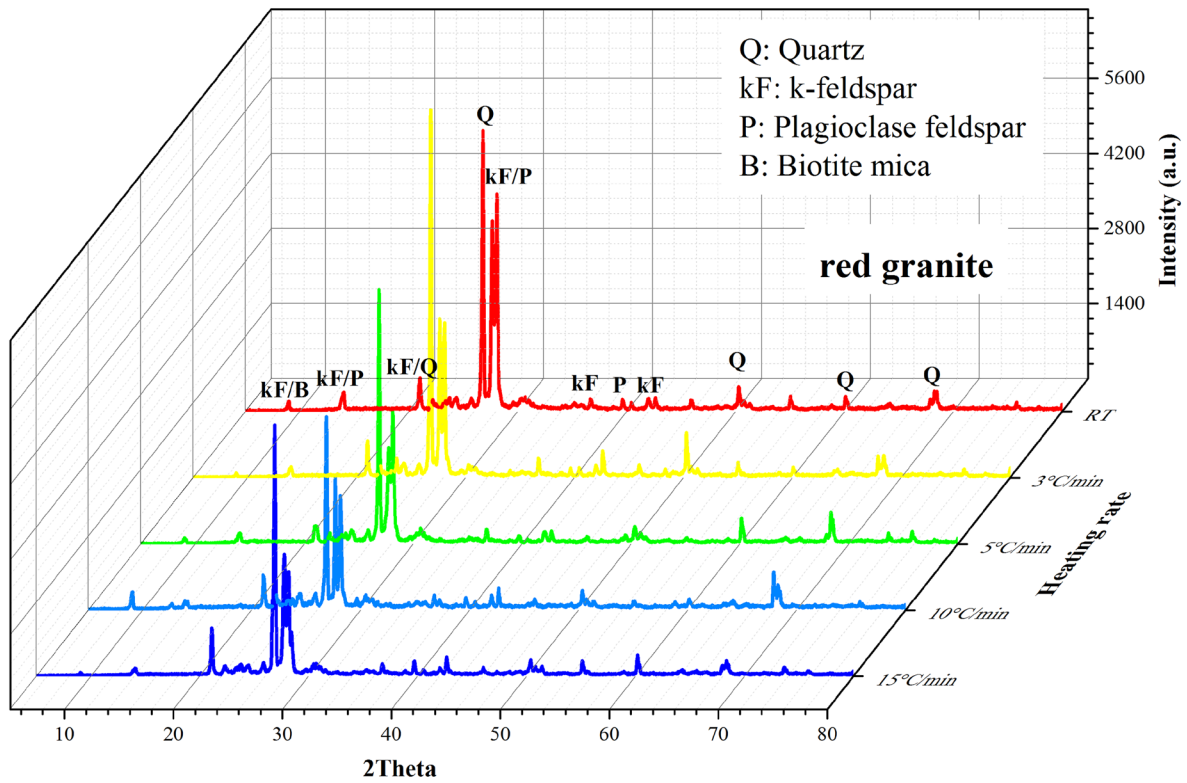

(b)

Fig. 19 X-ray diffraction spectra. **a** White granite. **b** Red granite

in contrast to the microcracks caused by following mechanical operations, which are the result of stress-driven. The eventual influence of microcracking on rock strength is entirely dependent on either the dominant role of thermally induced microcracks or the interaction between thermally induced and stress-induced microcracks. Then, the conflict between thermally induced microcracks' damage effect and their contribution to stress-induced microcrack inhabitation is comparatively poorly known. A scanning electron microscope (SEM) is used to analyze the detailed microstructure properties of crack patterns generated inside granite and fracture morphology under different thermal treatment conditions. Hence, SEM observations of macroscopic properties and fracture morphology under the tensile failure of coarse-grained red granite and fine-grain white granite are shown in Figs. 17 and 18. However, natural voids and pre-existing cracks are observed in RG and WG at room temperature as shown in Figs. 17a and 18a. At 3 and 5 °C/min heating rates, the different cracks including microcracks, large cracks, secondary cracks, and interconnected cracks appear in the internal structure of coarse grain red granite specimens as shown in Fig. 17b and c. But, the number and size of microcracks increase steeply because of the enlargement of thermal cracking caused by 10 and 15 °C/min heating rate treatment in coarse grain red granite as shown in Fig. 17d and e. This is due to the internal structure of feldspar and muscovite changes that crack expansion, dehydration, and voids occur (Sun et al. 2020). In contrast, when the heating rate increases from 3 and 5 °C/min, the internal structure is almost unchanged, but the number and size of cracks increase as the heating rate increases from 10 and 15 °C/min in fine-grain white granite as shown in Fig. 18b–e.

In this study, EDX (elemental dispersive spectroscopy) shows that the temperature (300 °C) conditions are not high enough to induce crack initiation or any physical and chemical reaction. The findings show that the samples predominantly consist of oxygen (O) and silicon (Si), suggesting quartz is the major mineral in the studied rock. It can be confirmed whether the effect of heat causes the observed difference in percentage elemental composition in the samples. The weight (%) and atomic percentage of elements of the studied samples are presented in Table 2. The grain expansion is considered to be the only response to heat treatment because the chemical reaction is inactive below the 300 °C temperature range (Wong et al. 2020).

XRD and XRF analysis

XRD is a common method for determining the mineral composition of materials. But, the main mineral compositions of granitoid are quite simple, and their quantities may be determined based on the order of chemical affinity and the percentage of molecular weight. It is also possible to correctly assess mineral element content in rocks using this technique so that the calculated results are more trustworthy. Because of this, both XRD and XRF tests were chosen for this study. The chemical compositions (expressed as a compound) of granitoid when exposed to thermal treatment with different heating rates are obtained through an XRF analysis. The 300 °C temperature range where chemical reactions are inactive is justified by XRD scattering as shown in Fig. 19 and XRF data are presented in Table 3.

Limitations and future work

Note that the main focus of the current study has been on how cracks form during heating and thermal expansion in granitoid. This does not indicate that cracking in thermally stressed granitoid is caused by cooling conditions. We also note that the mechanism of cracking is due to grain contraction during cooling conditions, which is hypothesized to be different from those formed in thermally stressed rocks and is a highly complex and nuanced topic (Browning et al. 2016). So, in the future, the behavior of cracking caused by grain contraction during the cooling process could be studied.

Table 3 Variation of chemical compositions

Heating rate (°C/min)	SiO_2	Fe_2O_3	K_2O	MgO	Na_2O	P_2O_5	TiO_2	MnO	Al_2O_3	CaO	LOI
WG_RT	74.79	1.24	4.46	0.18	2.99	0.07	0.08	0.03	11.84	1.22	1.97
3	74.74	1.18	4.70	0.15	2.84	0.06	0.08	0.03	11.74	1.08	1.86
5	75.88	1.31	4.56	0.17	2.77	0.06	0.08	0.04	11.75	1.19	0.99
10	75.83	1.23	4.48	0.15	2.90	0.06	0.08	0.03	11.84	1.08	0.77
15	75.60	1.08	4.47	0.15	2.85	0.06	0.07	0.03	11.73	1.18	1.57
RG_RT	74.19	1.28	4.76	0.10	3.84	0.05	0.12	0.01	11.93	0.94	1.24
3	75.78	0.93	4.90	0.07	3.55	0.05	0.08	0.01	11.88	0.86	1.47
5	74.83	0.90	4.87	0.09	3.78	0.05	0.09	0.00	11.77	0.90	1.16
10	69.86	2.85	5.43	0.63	3.68	0.16	0.41	0.04	13.78	1.71	1.16
15	75.90	0.87	4.90	0.09	3.80	0.05	0.09	0.00	11.82	0.89	1.46

Conclusions

In this study, indirect tension tests were conducted on two types of Jalore granitic rocks that had been heat-treated to 300 °C at different heating rate (3, 5, 10, and 15 °C/min) treatments. The effect of heating rate on thermomechanical performance in granitic specimens was also investigated. The major conclusions of this research are summarized as follows.

1. When the number of thermal cracks increases, the tensile strength, elastic modulus, and deformation modulus decrease, while failure strain increases. Thermal cracks develop after the heating rate threshold value, which lies between 3 and 5 °C/min. The heating rate of less than or equal to 5 °C/min should be used to avoid thermal shock damage.
2. The thermal expansion coefficient of coarse-grained red granite is higher than that of fine-grained white granite because it has a larger grain size and extreme heterogeneity. At heating rates of 3, 5, 10, and 15 °C/min, the thermal expansion coefficient of coarse-grained granite is 1.19, 1.21, 1.24, and 1.28 times larger than that of fine-grained granite.
3. The mineral, chemical, and elemental compositions of granite do not change significantly when heated to 300 °C at different heating rates.
4. Granite is an excellent natural barrier for blocking and preventing radioactive waste leakage. According to the data presented in this work, thermally induced and stress-induced microcracks were more readily visible in coarse-grained red granite, while less visible in fine-grained white granite. As a result, fine-grained white granite with good thermomechanical stability should be considered a suitable candidate as a host rock for India's high-level radioactive waste repository.

Supplementary Information The online version contains supplementary material available at https://doi.org/10.1007/s10064-022-02962-y.

Acknowledgements The first author wanted to express his gratitude to the Indian Institute of Technology Kanpur for providing financial support through the Postdoctoral Fellowship Program.

Declarations

Conflict of interest The authors declare no competing interests.

References

Bäckblom G, Martin CD (1999) Recent experiments in hard rocks to study the excavation response: implication for the performance of a nuclear waste geological repository. Tunn Undergr Space Technol 14(3):377–394

Backers T, Meier T, Gipper P, Stephansson O (2014) Rock mechanics - confidence of SKB's models for predicting the occurrence of spalling – main review phase 2014:10. Swedish radiation safety authority (Technical Note 49)

Birkholzer J, James H, Tsang CF (2012) Geologic disposal of high-level radioactive waste: status, key issues, and trends. Annu Rev Environ Resour 37:79–106

Browning J, Meredith P, Gudmundsson A (2016) Cooling-dominated cracking in thermally stressed volcanic rocks. Geophys Res Lett 43(16):8417–8425

Chaki S, Takarli M, Agbodjan WP (2008) Influence of thermal damage on physical properties of a granite rock: porosity, permeability, and ultrasonic wave evolutions. Constr Build Mater 22:1456–1461

Chang X, Zhang X, Dang F, Zhang B, Chang F (2022) Failure behavior of sandstone specimens containing a single flaw under true triaxial compression. Rock Mech Rock Eng 55(4):2111–2127

Chen S, Yang C, Wang G (2017) Evolution of thermal damage and permeability of Beishan granite. Appl Therm Eng 110:1533–1542

David C, Menendez B, Darot M (1999) Influence of stress-induced and thermal cracking on physical properties and microstructure of La Peyratte granite. Int J Rock Mech Min Sci 36:433–448

Dos Santos JPL, Rosa LG, Amaral PM (2011) Temperature effects on mechanical behaviour of engineered stones. Constr Build Mater 25:171–174

Dutt A, Saini MS, Singh TN, Verma AK, Bajpai RK (2012) Analysis of thermo-hydrologic-mechanical impact of repository for high-level radioactive waste in clay host formation: an Indian reference disposal system. Environ Earth Sci 66(8):2327–2341

Dwivedi RD, Goel RK, Prasad VVR, Sinha A (2008) Thermo-mechanical properties of Indian and other granites. Int J Rock Mech Min Sci 45:303–315

Ersoy H, Kolaylı H, Karahan M, Harputlu Karahan H, Sünnetci MO (2019) Effect of thermal damage on mineralogical and strength properties of basic volcanic rocks exposed to high temperatures. Bull Eng Geol Env 78(3):1515–1525

Fan LF, Gao JW, Wu ZJ, Yang SQ, Ma GW (2018) An investigation of thermal effects on micro-properties of granite by X-ray CT technique. Appl Therm Eng 140:505–519

Fan LF, Wu ZJ, Wan Z, Gao JW (2017) Experimental investigation of thermal effects on dynamic behavior of granite. Appl Therm Eng 125:94–103

Gautam PK, Dwivedi R, Kumar A, Kumar A, Verma AK, Singh KH, Singh TN (2021) Damage characteristics of Jalore granitic rocks after thermal cycling effect for nuclear waste repository. Rock Mech Rock Eng 54(1):235–254

Gautam PK, Jha MK, Verma AK, Singh TN (2019a) Evolution of absorption energy per unit thickness of damaged sandstone. J Therm Anal Calorim 136(6):2305–2318

Gautam PK, Jha MK, Verma AK, Singh TN (2020) Experimental study of thermal damage under compression and tension of Makrana marble. J Therm Anal Calorim 139(1):609–627

Gautam PK, Verma AK, Jha MK, Sarkar K, Singh TN, Bajpai RK (2016a) Study of strain rate and thermal damage of Dholpur sandstone at elevated temperature. Rock Mech Rock Eng 49(9):3805–3815

Gautam PK, Verma AK, Jha MK, Sharma P, Singh TN (2018a) Effect of high temperature on physical and mechanical properties of Jalore granite. J Appl Geophys 159:460–474

Gautam PK, Verma AK, Maheshwar S, Singh TN (2016b) Thermo-mechanical analysis of different types of sandstone at elevated temperature. Rock Mech Rock Eng 49(5):1985–1993

Gautam PK, Verma AK, Sharma P, Singh TN (2018b) Evolution of thermal damage threshold of Jalore granite. Rock Mech Rock Eng 51(9):2949–2956

Gautam PK, Verma AK, Singh TN, Hu W, Singh KH (2019b) Experimental investigations on the thermal properties of Jalore granitic rocks for nuclear waste repository. Thermochim Acta 681:178381

Guo TY, Wong LNY (2020) Microcracking behavior of three granites under mode I loading: insights from acoustic emission. Eng Geol 278:105823

Hajiabdolmajid V, Kaiser P, Martin CD (2003) Mobilised strength components in brittle failure of rock. Geotechnique 53(3):327–336

Hajpál M (2002) Changes in sandstones of historical monuments exposed to fire or high temperature. Fire Technol 38(4):373–382

Heuze FE (1981) On the geotechnical modelling of high-level nuclear waste disposal by rock melting. Lawrence Livermore National Laboratory (Report UCRL-53183)

Huang S, Xia KW (2015) Effect of heat-treatment on the dynamic compressive strength of Longyou sandstone. Eng Geol 191:1–7

Hudson JA, Bäckström A, Rutqvist J, Jing L, Backers T, Chijimatsu M, Christiansson R, Feng XT, Kobayashi A, Koyama T, Lee HS, Neretnieks I, Pan PZ, Rinne M, Shen BT (2009) Characterising and modelling the excavation damaged zone in crystalline rock in the context of radioactive waste disposal. Environ Geol 57(6):1275–1297

Hudson JA, Cosgrove JW, Kemppainen K, Johansson E (2011) Faults in crystalline rock and the estimation of their mechanical properties at the Olkiluoto site, western Finland. Eng Geol 117:246–258

IAEA (2009) Geological disposal of radioactive waste: technological implications for retrievability. IAEA (Nuclear Energy Series, No. NW-T-1.19)

Incroera FP, Dewitt DP, Bergman TL et al (2007) Fundamentals of heat and mass transfer. J. Wiley, New York

Isaka B, Gamage R, Rathnaweera T, Perera M, Chandrasekharam D, Kumari W (2018) An influence of thermally induced microcracking under cooling treatments: mechanical characteristics of Australian granite. Energies 6:1338

ISRM (1978) Suggested methods for determining the uniaxial compressive strength and deformability of rock materials. Int J Rock Mech Min Sci Geomech Abstr 16:137–140. https://doi.org/10.1016/0148-9062(79)91450-5

Krajcinovic D, Silva MAG (1982) Statistical aspects of the continuous damage theory. Int J Solids Struct 18(7):551–562

Kumari WGP, Ranjith PG, Perera MSA et al (2017) Temperature-dependent mechanical behaviour of Australian Strathbogie granite with different cooling treatments. Eng Geol 229:31–44

Li B, Ju F (2018) Thermal stability of granite for high temperature thermal energy storage in concentrating solar power plants. Appl Therm Eng 138:409–416

Lin W (2002) Permanent strain of thermal expansion and thermally induced microcracking in Inada granite. J Geophys Res Solid Earth 107:ECV-3

Liu S, Xu JY (2015) An experimental study on the physico-mechanical properties of two post-high-temperature rocks. Eng Geol 185:63–70

Maheshwar S, Verma AK, Singh TN, Bajpai RK (2015) Study of thermo-hydro-mechanical processes at a potential site of an Indian nuclear waste repository. J Earth Syst Sci 124(8):1693–1708

Nasseri MHB, Schubnel A, Young RP (2007) Coupled evolutions of fracture toughness and elastic wave velocities at high crack density in thermally treated Westerly granite. Int J Rock Mech Min Sci 44:601–616

Nasseri MHB, Tatone BSA, Grasselli G, Young RP (2009) Fracture toughness and fracture roughness interrelationship in thermally treated westerly granite. Pure Appl Geophys 166(5–7):801–822

Pai N, Feng J, Haijian S, Zequan H, Meng X, Yazhen Z, Dong W (2021) An investigation on the deterioration of physical and mechanical properties of granite after cyclic thermal shock. Geothermics 97:102252

Peng J, Rong G, Cai M, Yao MD, Zhou CB (2016) Comparison of mechanical properties of undamaged and thermal-damaged coarse marbles under triaxial compression. Int J Rock Mech Min Sci 83:135–139

Peng J, Rong G, Yao M, Wong LN, Tang Z (2019) Acoustic emission characteristics of a fine-grained marble with different thermal damages and specimen sizes. Bull Eng Geol Environ 78(6):4479–5449

Ramana YV, Sarma LP (1980) Thermal expansion of a few Indian granitic rocks. Phys Earth Planet Inter 22(1):36–41

Rathnaweera TD, Ranjith PG, Gu X, Perera MS, Kumari WG, Wanniarachchi WA, Haque A, Li JC (2018) Experimental investigation of thermomechanical behaviour of clay-rich sandstone at extreme temperatures followed by cooling treatments. Int J Rock Mech Min Sci 107:208–223

Renani HR, Martin CD (2018) Cohesion degradation and friction mobilization in brittle failure of rocks. Int J Rock Mech Min Sci 106:1–13

Rong G, Jun P, Ming C, Mengdi Y, Chuangbing Z, Song S (2018) Experimental investigation of thermal cycling effect on physical and mechanical properties of bedrocks in geothermal fields. Appl Therm Eng 141:174–185

Rossi E, Kant MA, Madonna C, Saar MO, Rudolf von Rohr P (2018) The effects of high heating rate and high temperature on the rock strength: feasibility study of a thermally assisted drilling method. Rock Mech Rock Eng 51(9):2957–2964

Sajid M, Arif M (2015) Reliance of physico-mechanical properties on petrographic characteristics: consequences from the study of Utla granites, north-west Pakistan. Bull Eng Geol Env 74(4):1321–1330

Sajid M, Coggan J, Arif M, Andersen J, Rollinson G (2016) Petrographic features as an effective indicator for the variation in strength of granites. Eng Geol 202:44–54

Shang XJ, Zhang ZZ, Xu XL et al (2019) Mineral composition, pore structure, and mechanical characteristics of pyroxene granite exposed to heat treatments. Mineral 9:553

Shao S, Wasantha PL, Ranjith PG, Chen BK (2014) Effect of cooling rate on the mechanical behavior of heated Strathbogie granite with different grain sizes. Int J Rock Mech Min Sci 70:381–387

Shi X, Jing H, Yin Q, Zhao Z, Han G, Gao Y (2020) Investigation on physical and mechanical properties of bedded sandstone after high-temperature exposure. Bull Eng Geol Env 79(5):2591–2606

Shu R, Huang L, Zhi X, Han Z, Lai Y, Li H, Wang C (2022) Damage characteristic of thermal shock on the physical and dynamic compressive properties of granite. Geofluids 2022:1623883

Sizgek GD (2004) Three-dimensional thermal analysis of in-floor type nuclear waste repository for a ceramic waste form. Nucl Eng Des 235(1):101–109

SKB (2004) Programme for research, development and demonstration of methods for the management and disposal of nuclear waste, including social science research, SKB TR-04-21, Svensk Karnbranslehantering AB, Stockholm

Sun Q, Geng J, Zhao F (2020) Experiment study of physical and mechanical properties of sandstone after variable thermal cycles. Bull Eng Geol Env 79(7):3771–3784

Tsang CF, Barnichon JD, Birkholzer J, Li XL, Liu HH, Sillen X (2012) Coupled thermo-hydro-mechanical processes in the near field of a high level radioactive waste repository in clay formations. Int J Rock Mech Min Sci 49:31–44

Verma AK, Gautam PK, Singh TN, Bajpai RK (2015) Discrete element modelling of conceptual deep geological repository for high-level nuclear waste disposal. Arab J Geosci 8(10):8027–8038

Wang F, Frühwirt T, Konietzky H, Zhu Q (2019) Thermo-mechanical behaviour of granite during high-speed heating. Eng Geol 260:105258

Wang F, Konietzky H (2019) Thermo-mechanical properties of granite at elevated temperatures and numerical simulation of thermal cracking. Rock Mech Rock Eng 52(10):3737–3755

Wang J (2010) High-level radioactive waste disposal in China: update 2010. J Rockmech Geotech Eng 2:1–11

Wang J (2014) On area-specific underground research laboratory for geological disposal of high-level radioactive waste in China. J Rock Mech Geotech Eng 6:99–104

Wang XQ, Schubnel A, Fortin J, Gueguen Y, Ge HK (2013) Physical properties and brittle strength of thermally cracked granite under confinement. J Geophys Res Solid Earth 118:6099–6112

Wong LNY, Zhang Y, Wu Z (2020) Rock strengthening or weakening upon heating in the mild temperature range? Eng Geol 272:105619

Wu X, Huang Z, Cheng Z, Zhang S, Song H, Zhao X (2019) Effects of cyclic heating and LN2-cooling on the physical and mechanical properties of granite. Appl Therm Eng 156:99–110

Wu Z, Zhang C (1996) Study on rock damage model and mechanical properties under uniaxial loading. Chin J Rock Mech Eng 15(1):55–61

Xi DY (1994) Physical characteristics of mineral phase transition in the granite. Acta Min Sinica 14(3):223–227

Yang SQ, Hu B (2018) Creep and long-term permeability of a red sandstone subjected to cyclic loading after thermal treatments. Rock Mech Rock Eng 51:2981–3004

Yılmaz NG, Goktan RM, Kibici Y (2011) Relations between some quantitative petrographic characteristics and mechanical strength properties of granitic building stones. Int J Rock Mech Min Sci 48(3):506–513

Yin W, Feng Z, Zhao Y (2021) Effect of grain size on the mechanical behaviour of granite under high temperature and triaxial stresses. Rock Mech Rock Eng 54(2):745–758

Yong C, Wang CY (1980) Thermally induced acoustic emission in Westerly granite. Geophys Res Lett 7(12):1089–1092

Zhang W, Sun Q, Hao S, Geng J, Lv C (2016) Experimental study on the variation of physical and mechanical properties of rock after high temperature treatment. Appl Therm Eng 98:1297–1304

Zhao XG, Wang J, Chen F, Li PF, Ma LK, Xie JL, Liu YM (2016) Experimental investigations on the thermal conductivity characteristics of Beishan granitic rocks for China's HLW disposal. Tectonophysics 683:124–137

Zhao XG, Zhao Z, Guo Z, Cai M, Li X, Li PF, Wang J (2018) Influence of thermal treatment on the thermal conductivity of Beishan granite. Rock Mech Rock Eng 51(7):2055–2074

Zhao Z (2016) Thermal influence on mechanical properties of granite: a microcracking perspective. Rock Mech Rock Eng 49:747–762

Zuo JP, Wang JT, Sun YJ, Chen Y, Jiang GH, Li YH (2017) Effects of thermal treatment on fracture characteristics of granite from Beishan, a possible high-level radioactive waste disposal site in China. Eng Fract Mech 182:425–437

Springer Nature or its licensor holds exclusive rights to this article under a publishing agreement with the author(s) or other rightsholder(s); author self-archiving of the accepted manuscript version of this article is solely governed by the terms of such publishing agreement and applicable law.